THESIS FOR THE DEGREE OF DOCTOR OF PHILOSOPHY

Fundamental studies of catalytic systems for diesel emission control

Aging and sulfur treatment of a DOC, spatial investigation and kinetic modeling of NO_x reduction by ammonia

XAVIER AUVRAY

Department of Chemical and Biological Engineering
CHALMERS UNIVERSITY OF TECHNOLOGY
Göteborg, Sweden 2013

Fundamental studies of catalytic systems for diesel emission control
Aging and sulfur treatment of a DOC, spatial investigation and kinetic modeling of NO_x reduction by ammonia

XAVIER AUVRAY

ISBN: 978-91-7385-942-4

Doktorsavhandlingar vid Chalmers tekniska högskola
Ny Serie nr. 3623
ISSN: 0346-718X

Department of Chemical and Biological Engineering
Competence Centre for Catalysis
Chalmers University of Technology
SE-412 96 Göteborg
Sweden
Telephone +46 (0)31 772 1000

Chalmers Reproservice
Göteborg, Sweden 2013

Fundamental studies of catalytic systems for diesel emission control

Aging and sulfur treatment of a DOC, spatial investigation and kinetic modeling of NO_x reduction by ammonia

XAVIER AUVRAY
Department of Chemical and Biological Engineering
Chalmers University of Technology

Abstract:

Due to global lean exhaust gas and new emission regulations, exhaust aftertreatment systems of diesel engines are more and more sophisticated and composed of a series of catalytic units. In the present work, two of these catalytic systems were studied with different approach. A model diesel oxidation catalyst (DOC), used to convert nitric oxide into nitrogen dioxide and hydrocarbons and CO into CO_2, was examined in flow reactor experiments. A Cu-exchanged zeolite catalyst, devoted to the lean NO_x reduction by ammonia was studied with SpaciMS in operating conditions.

Since longevity and resistance to poisoning are two major challenges for automotive catalysts, the effect of thermal aging in reactive atmosphere on NO oxidation activity was addressed and correlated to platinum dispersion. Our experiments revealed the promotion of Pt sintering by SO_2 as well as the improvement of oxidation ability. Sintering in argon to obtain similar Pt dispersion did not result in similar performance indicating the important role of aging atmosphere in subsequent activity. The DOC was subjected to SO_2 treatment in order to characterize the sulfur species formed during SO_2 poisoning and their impact on the oxidation of NO and C_3H_6. Two types of sulfur species that differ in stored amount and impact on the activity were distinguished by TPR experiment. However, both have a detrimental effect on the DOC performance. Finally, modification of the DOC formulation by incorporation of acidity enhancer groups was carried out. The introduction of chlorine and sulfate to increase the acidic nature of the support yielded suppression of catalyst deactivation due to platinum oxide formation. However, this effect disappeared after aging and subsequent TPR to 800°C, suggesting a loss of these acidity-promoters.

The study of the NO_x reduction catalyst was performed to evaluate its activity, NH_3 storage capacity and NH_3 and NO oxidation ability. Intra-catalyst measurements were achieved with SpaciMS at Oak Ridge National Laboratory. This technique provides insight of the reaction evolution throughout the monolithic catalyst and showed the diminishing of the zone used for SCR reaction as the temperature increased from 200 to 400°C. The intra-catalyst concentration profiles are valuable data acquired in realistic flow and temperature conditions and was utilized to develop a kinetic model for standard NH_3-SCR. The model accounts for the N_2O production according to two routes and predicts well the transient phenomena resulting from changes in gas composition.

Keywords: NO oxidation, DOC, NH_3 SCR, aging, sulfur, SpaciMS, hysteresis, Pt/Al_2O_3, kinetic modeling, catalyst acidity

List of publications:

Paper I

The Effect Gas Composition During Thermal Aging On The Dispersion And NO Oxidation Activity Over Pt/Al_2O_3 Catalysts.

Auvray X.; Pingel T.; Olsson E.; Olsson L.

Applied Catalysis B: Environmental, 129 (2013) pp. 517-527.

Paper II

Sulfur Dioxide Exposure: A Way To Improve The Oxidation Catalyst Performance

Auvray X.; Olsson L.

Industrial & Engineering Chemistry Research, 52, 41, (2013) pp. 14556-14566

Paper III

Effect Of Enhanced Support Acidity On The Sulfate Storage And The Activity Of Pt/γ-Al_2O_3 For NO Oxidation And Propylene Oxidation

Auvray X.; Olsson L.

Catalysis Letters, accepted for publication (2013)

Paper IV

Local Ammonia Storage And Ammonia Inhibition In A Monolithic Copper-Beta Zeolite SCR Catalyst

Auvray X.; Partridge W. P.; Choi J. S.; Pihl J. A.; Yezerets A.; Kamasamudram K.; Currier N. W.; Olsson L.

Applied Catalysis B: Environmental, 126 (2012) pp. 144-152.

Paper V

Kinetic Modeling Of NH_3-SCR Over A Supported Cu Zeolite Catalyst Using Axial Species Distribution Measurements

Auvray X.; Partridge W. P.; Choi J. S.; Pihl J. A.; Coehlo F.; Yezerets A.; Kamasamudram K.; Currier N. W.; Olsson L.

In manuscript

Contribution to the papers:

Paper I

I synthesized the catalysts and conducted all the reactor experiments. I interpreted the results with my co-authors and was responsible for writing the manuscript.

Paper II

I synthesized the catalysts and conducted all the experiments. I interpreted the results together with my co-author and was responsible for writing the manuscript.

Paper III

I designed and synthesized the catalysts and conducted all the experiments. I interpreted the results with my co-author and was responsible for writing the manuscript.

Paper IV

I performed the experiments, analyzed the results together with my co-authors and wrote the first manuscript.

Paper V

I performed the experiments and simulations, analyzed the results together with my co-authors and was responsible for writing the manuscript.

Contents

Chapter 1

Introduction – emission control catalysis

The massive emission of CO_2 started with the industrial era has led to a threatening global warming due to CO_2 greenhouse effect. Decisions were taken in order to decrease the global CO_2 emissions and, as a major emitter, the transportation sector has been targeted. In addition, with the oil resources depletion and the always-increasing oil demand, a great effort has been devoted to develop more fuel-efficient engines like diesel and lean-burn gasoline engines. For a more complete reaction, these engines work at higher air-to-fuel ratio which lowers the fuel consumption and also reduces carbon dioxide release. As a consequence, the nature of the exhaust gas is also modified and is now globally oxidizing due to excess oxygen in the engine feed. This characteristic has a major impact on the catalytic treatment of the exhaust. Pollution caused by combustion emissions has been a concern for a long time and led to the introduction of emission regulations. In 1967, the United States adopted the Clean Air Act to reduce vehicle emissions. To satisfy more stringent regulations, oxidation catalysts, responsible for the carbon monoxide (CO) and hydrocarbons (HC) emission control, were commercialized in the mid-1970s. In the 1980s, the three-way catalyst technology (TWC) was developed to simultaneously reduce the emission HC, CO and NO_x, i.e. NO and NO_2 for gasoline engine applications. TWC utilizes CO and HC to reduce NO_x and is efficient within a narrow air-to-fuel ratio window centered on 14.6, which corresponds to the stoichiometric operation of the engine. This technology requires an accurate control of the fuel injection and air intake, which is achieved by measuring the oxygen concentration of the exhausts, thus providing feedback to the injection control unit. Diesel and lean-burn engines do not operate on this critical window, and therefore the TWC can only oxidize HC and CO but cannot handle NO_x in these oxidizing conditions.

The release of NO_x in the atmosphere represents a health hazard in urban area. NO can react with other chemical species to form very toxic compounds such as NO_2 and ozone. NO_x is one of the main components of the brownish haze called “smog” that also contains particulate matters, hydrocarbons and SO_2. Under the action of sunlight, the extremely active ozone forms by reaction between NO_x and HC with severe consequence on air quality. The reactive nature of ozone can provoke respiratory problems such as asthma, attack lung tissue and it inhibits the growth of plants. On a more global level, NO_x are also able to react with water to form nitric acid yielding acid rains. Therefore, more restrictive emission regulations have been introduced and forced the design of new catalytic systems to reduce NO_x produced by diesel and lean-burn vehicles. Two processes aiming at reducing vehicle NO_x emissions have emerged in the 90’s.

The lean NO_x-trap (LNT) technique is based on cycling the operating regime of the engine between fuel-lean and fuel-rich. During the lean period, NO_x are stored on the catalyst designed to trap NO_x in form of surface nitrates thanks to an alkaline metal like barium. When the catalyst cannot trap 100 % of the NO_x, the regime is switched to rich mode by increasing the ratio of fuel/oxygen for a few seconds. Thus the excess of unburned fuel in the exhaust is used as a reductant to convert stored NO_x into N_2 and H_2O. This technique is sensitive to sulfur and requires a very precise control of the engine and the catalyst and the rich periods penalize the fuel economy.

The second method is the selective catalytic reduction (SCR) of NO_x by injecting a reductant in the gas stream upfront the catalyst. The mixture containing NO_x and the reducing agent flows to a catalyst, on which the reduction of NO_x into N_2 and H_2O occurs. Many types of catalysts and reductants have been studied. The fuel can be used as a source of hydrocarbons for HC-SCR, which led to many studies [1, 2]. NH_3 is also able to reduce selectively NO [3] and can be produced in situ by the decomposition of a urea solution. NH_3-SCR does not involve extra fuel consumption but demands a tank to store the urea solution onboard as well as an accurate dosing system. The addition of a subsequent ammonia slip catalyst (ASC) to control the excess NH_3 that may slip out of the vehicle is also a necessity.

As for gasoline engines, the after-treatment system of diesel engines includes an oxidation unit, but with a slightly different function. Besides oxidizing CO and HC, the specific role of a diesel oxidation catalyst (DOC) consists in converting NO into NO_2, which is a suitable oxidant to burn the soot trapped by the diesel particulate filter (DPF). NO_2 is not only used to regenerate the DPF, it plays an important role in the two aforementioned NO_x abatement processes. Indeed, NO_2 adsorbs more readily than NO, enhancing the trapping performance of the LNT catalyst. The SCR is also improved by the presence of NO_2 up to a NO_2/NO ratio of 1.

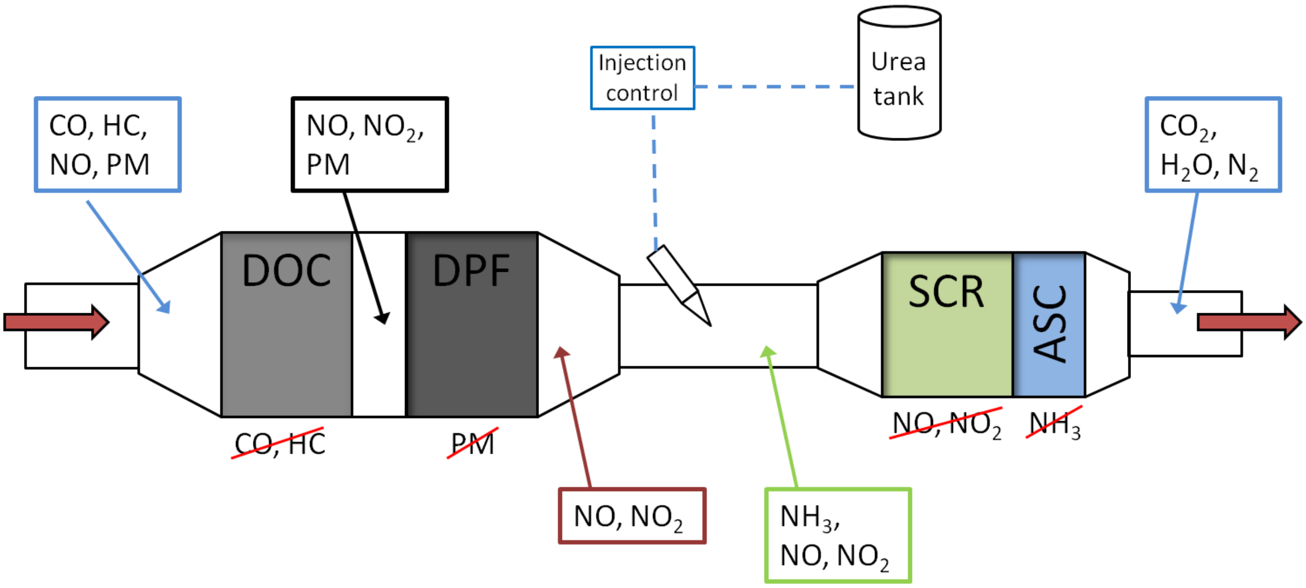

Figure 1: Combination of catalysts to reduce emissions of diesel vehicles.

In operating conditions, catalysts are exposed to variable temperature and gas composition that may alter their structure and performance. The exhaust gas temperature attained downstream the DPF can be very high due to the heat generated by the soot combustion. High temperature exposure causes metal agglomeration and structural transition of the support material leading to the decrease in catalytic surface area and deactivation. Fuel and lube oil contain small amount of inorganic elements that end up in the exhausts and affect the catalyst. Despite the progress made in de-sulfurization of fuel, sulfur remains a major source of catalyst poisoning. It is oxidized in the engine chamber to form SO_2, which has a great affinity with conventional catalytic materials and blocks the active sites by covering them. SO_2 poisoning is particularly hindering on LNT because it forms stable sulfates with the NO_x-adsorbing material, thus gradually decreasing the NO_x-storage capacity of the LNT [4]. Phosphorous, sodium, zinc, magnesium and calcium figure also among potential poisons for the catalyst. A great interest has been shown in studies of thermal and chemical deactivation in order to understand the underlying mechanism and design more durable catalysts.

Chapter 2

Objectives

The major part of this thesis has been dedicated to the study of a typical oxidation catalyst in aging conditions (Paper I-III). The effect of thermal treatment coupled to chemical exposure on the NO oxidation activity was investigated in Paper I. The goal was to characterize the platinum sintering of a 1 wt.% Pt/Al_2O_3 catalyst aged in various atmosphere in a flow reactor. The Pt dispersion was measured by CO chemisorption and the particles were directly observed by transmission electron microscopy (TEM). The characterization was completed by the BET surface area measurement and the activity test for NO oxidation.

SO_2 is a typical compound contained in the vehicle exhausts and showed remarkable ability to promote platinum sintering. The catalyst treated in this way interestingly showed an increased activity towards NO oxidation in Paper I. A more detailed study focused on the effect of SO_2 exposure was then conducted in order to evaluate the influence and stability of the sulfur adsorbates formed during aging and their interactions in subsequent reactions. Since the DOC mission is to oxidize both NO and hydrocarbons, the activity test was extended to propene oxidation. The results of this work are summarized in Paper II.

The formation of platinum oxides during NO oxidation has been noted in Paper I and II and credited with the catalyst deactivation and inverse hysteresis phenomenon. The acidity enhancement of the catalyst as a mean to suppress the Pt oxide formation was investigated in close relationship with the effect of sulfation treatment. The results are reported in Paper III.

The second part of this thesis deals with the selective catalytic reduction (SCR) of NO_x using NH_3 as reducing agent. Intra-catalyst gas analysis was performed with a SpaciMS to determine the spatial concentration profiles of the components involved in key reactions occurring on the SCR catalyst. The activity of a copper-exchanged zeolite catalyst was measured for NO oxidation, NH_3 oxidation and NH_3-SCR. Ammonia storage was also characterized since ammonia storage capacity is a crucial parameter for the NH_3-SCR technology. Indeed the dosing of NH_3 injection in the exhausts must take into account the stored ammonia, which also participates to the NO_x reduction. The results and the conclusions drawn from the spatially-resolved data are reported in Paper IV.

SpaciMS is an excellent tool to measure intra-catalyst gas composition and to sample the gas flow at several positions along the monolithic sample, giving a picture of the reaction rates. This type of data is therefore invaluable to study the kinetics of a reaction and is appropriate to use when developing kinetic models. The objective of the study presented in Paper V was to use the spatial data collected with SpaciMS in Paper IV in order to develop a global kinetic model for the NH_3-SCR process.

Chapter 3

Diesel Oxidation Catalyst

Oxidation catalysts were first used on spark-ignited gasoline engines to oxidize carbon monoxide and hydrocarbons. Diesel vehicles did not need such technology at that moment due to their already low CO and HC emissions. However with more stringent emission standards, the utilization of oxidation catalyst was extended to diesel applications. Diesel oxidation catalysts (DOC) have the additional task to convert NO into NO_2, which participates in particulate filter regeneration and improves the NO_x reduction process. DOCs are noble metal based catalysts; they typically contain Pt and Pd dispersed on high surface area supports like metal oxides. Commercial catalysts often contain additives that improve their thermal stability and durability or provide a promoting function such as oxygen storage capacity.

3.1. NO oxidation over Pt

3.1.1. Chemistry and thermodynamics

The oxidation of NO is an exothermic reaction, the standard enthalpy of which is -57.19 kJ/mol. The stoichiometry of the global reaction is given by equation (3.1):

$$\mathrm{NO} + \frac{1}{2}\,\mathrm{O_2} \leftrightarrow \mathrm{NO_2} \qquad (3.1)$$

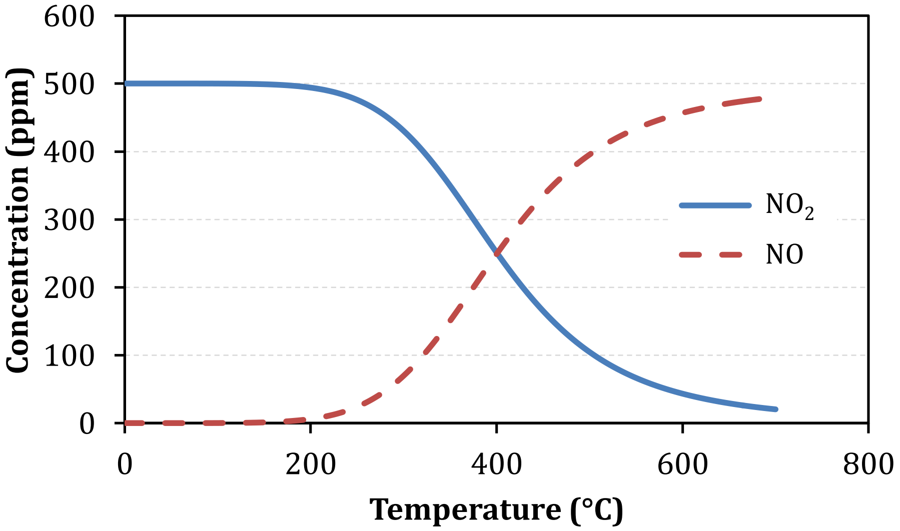

Figure 2: NO and NO_2 concentrations at thermodynamic equilibrium for a gas containing initially 8% O_2 and 500ppm NO.

As shown in Figure 2, at low temperature, the most stable species is nitrogen dioxide and the reaction (3.1) is favored. Conversely, the reaction is thermodynamically limited at high temperature. The catalyst should therefore be particularly active at low temperature. The gas composition plays a significant role in the conversion. Després et al. [5] noted the increase of NO conversion when the concentration of oxygen was increased. In contrary, high NO concentration led to low NO conversion. Kinetic studies [6, 7] report a global reaction order near 1 for O_2 and NO and near -1 for NO_2 indicating significant NO_2 inhibition [5, 8]. The value of activation energy and the catalytic mechanism used to model the reaction differ in the literature. The model developed by Olsson et al. [9, 10] describes the experiments equally well with the Langmuir-Hinshelwood model, which considers the surface reaction between adsorbed atomic oxygen and adsorbed NO, as with the Eley-Rideal model [10], which implies reaction between adsorbed oxygen and gas phase NO. However, to describe and include the NO_2 decomposition, which requires two adjacent surface sites, the Langmuir-Hinshelwood model was preferred. Due to a low NO adsorption above 200°C, Crocoll et al. used the Eley-Rideal mechanism for NO oxidation [11]. In contrary, Bhatia et al. [8] found that NO coverage was significant at low temperature and therefore should be included in kinetic models. In the model by Mulla et al. [6], the adsorption of molecular dioxygen was considered to be the rate-determining step. In this model, the apparent activation for NO oxidation was found to be 82 kJ/mol.

The particle size affects greatly the reaction rate and the conclusions of numerous studies [6, 12-18] suggest that larger particles have a higher intrinsic activity, evidenced by a higher turn-over rate (rate of moles of NO converted per Pt site). The reason commonly invoked is the greater resistance towards oxidation of the larger particles. Indeed, Wang and coworkers [19] demonstrated that the NO oxidation activity was lower on platinum oxides than on metallic platinum, supported by a higher energy barrier for NO adsorption and O_2 dissociation on PtO_2. Platinum oxidation is discussed in more detail in section 3.1.3. Matam et al. [20] suggested that particle morphology played an even more important role than particle size in the NO oxidation activity. They determined the rates for two aged catalysts; the one with higher dispersion presented the higher normalized rate constant, owing to more active particle morphology. They concluded that cuboctahedral morphology was the best configuration compared to truncated cubic and spherical Pt particles.

3.1.2. Deactivation factors

During NO oxidation, Pt/Al_2O_3 catalysts are prone to deactivate. This fact has been evidenced by the formation of an inverse hysteresis when the catalysts are successively heated and cooled during NO oxidation conditions [21-23]. The conversion obtained during the cooling was lower than the one measured during initial heating (Figure 3), indicating significant deactivation. Time-on-stream experiments (Figure 4) have also shown the decrease of NO conversion during isothermal step [14, 21]. Most of the authors who have investigated this phenomenon assigned the deactivation of the reversible formation of platinum oxide in operating conditions [6, 21]. The production of NO_2, known to be a powerful oxidant, as well as the high oxygen concentration is a factor enabled to explain the platinum reversible oxidation. Hauff et al. [21] showed that NO_2 had no influence on catalyst deactivation in presence of 12 % O_2, suggesting that oxygen has a significant responsibility in platinum oxidation.

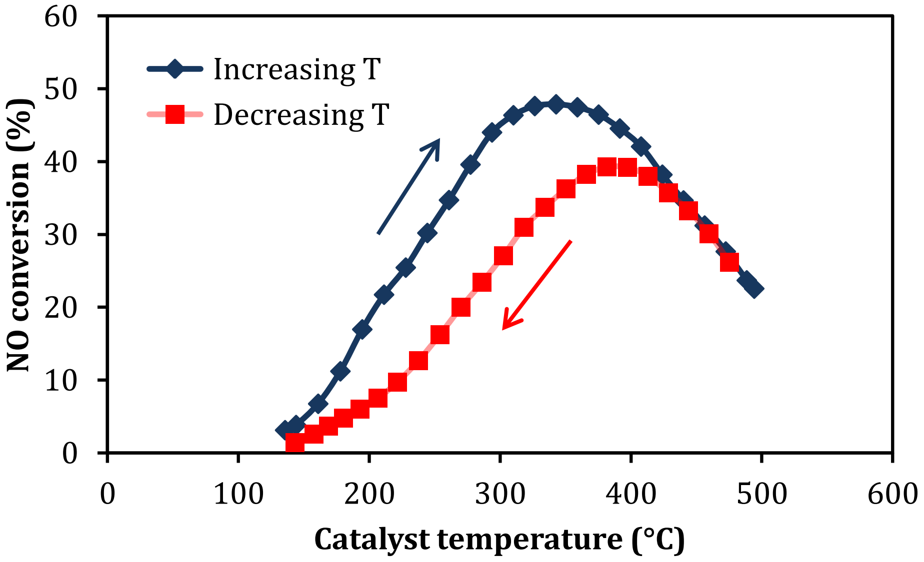

Figure 3: Hysteresis phenomenon during NO oxidation over Pt/Al_2O_3 (500ppm NO + 8% O_2 + 5% H_2O).

The kinetic study of Mulla et al. [7] pointed out the negative effect of NO_2 evidenced by the increase of the apparent activation energy, from 39 kJ/mol to 82 kJ/mol, due to the presence of NO_2 in the feed. They also determined by CO titration that the oxygen uptake of the catalyst was higher when it had been exposed to the reaction mixture (NO + O_2) than to oxygen [6]. The oxygen uptake was even higher upon exposure to NO_2 + O_2 which indicates the oxidation of platinum during activity measurement. The XPS results by Olsson and Fridell [14] depicted the formation of platinum oxide, enhanced by the presence of barium. Després et al. [5] also detected platinum oxide after pretreatment with O_2 and NO_2. Several studies demonstrated the negative effect of NO_2 on the reaction rate. The catalytic oxidation of NO on Pt-based catalysts is therefore self-inhibited. The interaction between dioxygen and the platinum is a crucial area in NO oxidation studies on platinum because oxygen dissociation on Pt surface is an important step in the catalytic process but, on the other hand, the strong oxygen-Pt interaction and oxygen diffusion in platinum particle cause deactivation. This is discussed in the next section.

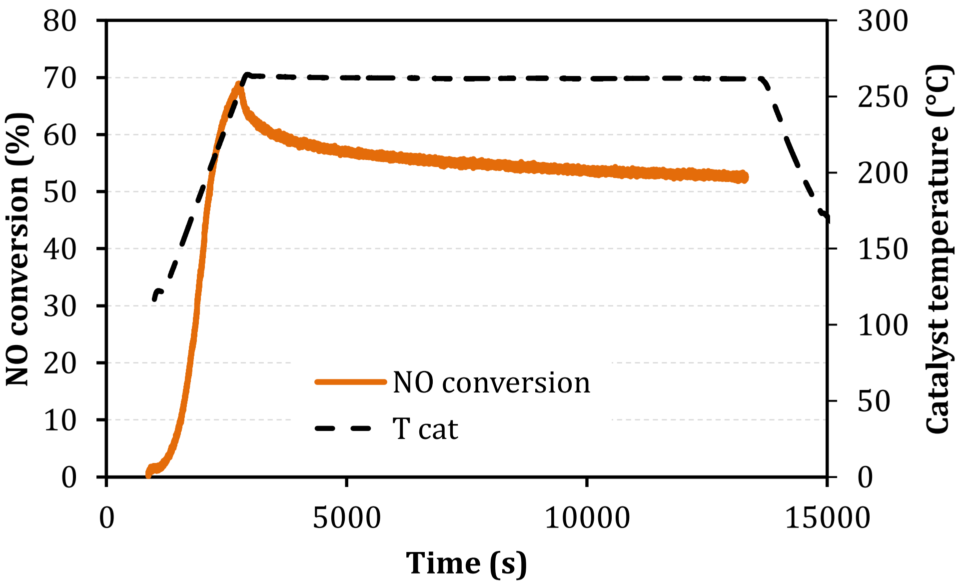

Figure 4: Catalyst deactivation with time on stream (3h) at 260°C in activity test conditions (500ppm NO, 8% O_2, 5% H_2O).

3.1.3. Oxygen adsorption and platinum oxidation

NO oxidation requires weakly bound oxygen on the surface [24]. However, on a clean Pt surface, oxygen forms stable bond with Pt. The increase of oxygen coverage increases the repulsive interaction between adsorbed O, creating more reactive oxygen. The weakening of Pt-O bond can also be achieved by an elevation of the temperature. Mudiyanselage et al. [24] evaluated the minimum oxygen coverage at 0.28 monolayer in order to produce this weakly bound oxygen. Ovesson et al. [25] calculated that repulsive lateral interactions between oxygen atoms and NO were necessary to render the NO oxidation exothermic.

Adsorbed oxygen is necessary for the reaction but in oxidizing environment, platinum oxides can form and deactivate the catalyst. The studies by Wang and Yeh [26, 27] on the oxidation of platinum nanoparticles give a valuable insight on the platinum dynamics in presence of O_2. Their calorimetric and gravimetric measurements revealed the different phases in the oxidation mechanism. At low temperature (<300 K), oxygen adsorbs on the surface with a high adsorption enthalpy. At higher temperature (300 < T < 750 K), the oxygen uptake per surface Pt increases and the heat of adsorption decreases, indicating greater oxidation and formation of surface Pt oxide. According to Wang and Yeh [26, 27], the stoichiometry of the surface platinum oxide depends on the particle size. For smaller particles (d<1.3 nm), the observed O/Pt^s ratio indicates that Pt^sO_2 was formed while Pt^sO was created on larger particles (d>2.0 nm). Finally at T>800 K, oxygen and/or platinum dioxide desorption occurs. Briot et al. [28] formulated a relationship between Pt particle size and adsorbed oxygen reactivity. Their calorimetric measurements showed a lower heat of oxygen adsorption on sintered catalysts accompanied with a higher TOR for methane oxidation. Furthermore, the reaction between H_2 and adsorbed oxygen occurred at lower temperature on the sintered catalyst implying higher reactivity of oxygen on larger particles. McCabe et al. [29] studied the passivating oxidation of platinum. The independence of oxygen uptake with oxygen pretreatment duration and temperature and the presence of both metallic Pt and Pt oxide signature in EXAFS spectra led the authors to conclude that only the platinum surface layer was subjected to oxidation. McCabe et al. also noted a relationship between Pt oxidation and particle size. It was found that small particles were reduced at higher temperature than larger particles, suggesting the higher stability of platinum oxide on small particles. It has been later confirmed that the heat of oxygen adsorption on Pt linearly decreases with the increase of particle size [26]. The size-dependent stoichiometry of Pt oxide measured by McCabe et al. [29] and Wang and Yeh [26, 27] are in agreement. The formation of less stable oxide on larger particle can explain the higher activity of sintered catalysts discussed in the section 3.1.1 and evidenced in Paper I and Paper II.

3.1.4. Interaction with other compounds

The NO oxidation, like most of catalytic reactions, is sensitive to chemical compounds present in the reactive gas mixture due to the more intense competition for adsorption sites on the catalyst. Since vehicle exhausts contain a wide variety of components, it is necessary to study their individual effect on the reaction of interest. The effect of the most common chemicals in automotive application such as water, HC, CO and CO_2 has been investigated. Other compounds such as SO_2, P and Ca, present in smaller quantities in automotive exhausts, have raised interest due to their major effect on catalytic systems.

The presence of propene inhibits the NO oxidation due to competitive adsorption and consumption of the produced NO_2 as oxidant for the propene oxidation reaction [30-32]. As a consequence NO oxidation is suppressed at temperature below the C_3H_6 combustion light-off temperature. Propane and dodecane hinder the oxidation of NO over Pt/Al_2O_3 as reported by Olsson et al. [33]. NO_x consumption was also observed when the gas flow contained dodecane, suggesting the occurrence of lean NO_x reduction by HC. The absence of this reaction in the case of propane indicates that the hydrocarbon chain length plays a selective role in the NO_x reduction. In the same manner, CO completely inhibits NO oxidation on Pt/Al_2O_3 until its total oxidation into CO_2 [21], which then facilitates the adsorption of NO. In a simulation, Crocoll et al. [11] calculated a high CO coverage and measured with DRIFT a strong adsorption of CO on Pt, resulting in a severe inhibition of NO oxidation. However, on Pt/TiO_2 catalyst, Irfan et al. [34, 35] observed the NO oxidation promotion by CO, which was attributed to the reduction of oxidized Pt by CO.

The influence of the most abundant compounds, namely CO_2 and H_2O, on NO oxidation has been investigated [11, 33]. CO_2 does not affect NO oxidation, which is supported by a theoretical low CO_2 coverage [11]. The addition of H_2O in the typical NO oxidation gas mixture decreases the NO_2 production [11, 33]. In addition, a puff of NO was detected when water was switched on [33]; indicating the replacement and release of adsorbed NO by H_2O. The detrimental effect of 5 % H_2O and 500 ppm C_3H_6 on the NO oxidation activity of Pt/Al_2O_3 catalyst is evidenced in Figure 5.

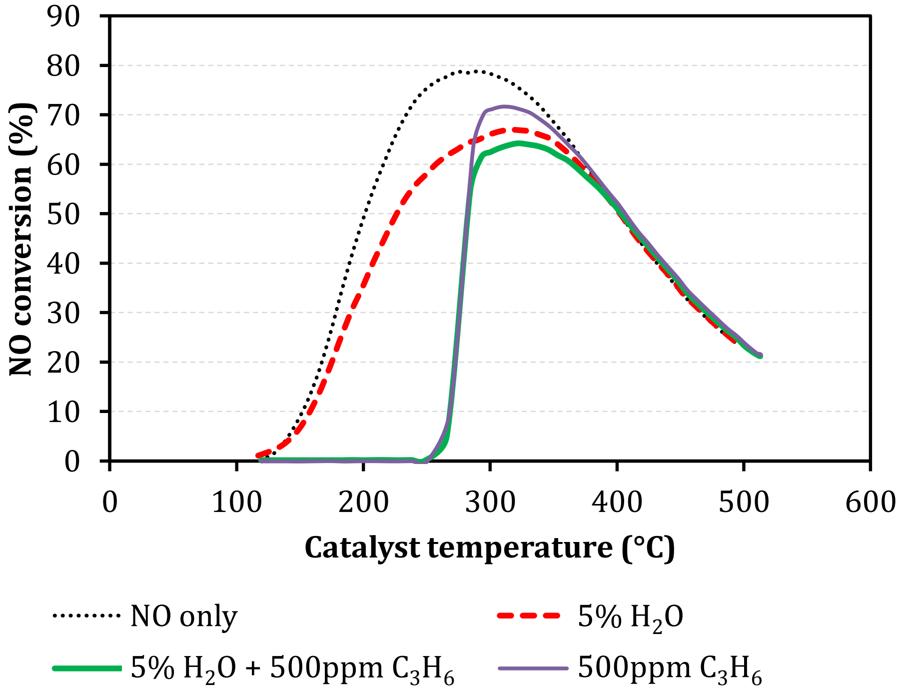

Figure 5: Effect of H_2O and C_3H_6 on NO oxidation over Pt/Al_2O_3 (500ppm NO, 8% O_2, 5°C/min).

3.2. Hydrocarbon oxidation

The first function of an automotive oxidation catalyst is to oxidize hydrocarbons and carbon monoxide that can remain in the exhausts into CO_2. Owing to its strong toxicity, CO must not be produced by HC combustion, which means that catalysts used must be selective to CO_2. Hydrocarbons represent a large group of molecules presenting different stability. Methane, for instance, is highly stable because its C-H bonds are difficult to break up. This is also the case for saturated HC (alkanes or paraffins) with short carbon chain. Unsaturated HC (alkenes or olefins), such as propene (called also propylene), are characterized by a C=C double bond that confers them a higher reactivity than alkanes. The high electron density of propene favors the interaction and adsorption on a catalytic surface. After exposure of Pt/Al_2O_3 to C_3H_6 and C_3H_8, Yao et al. [36] observed no propane chemisorption but a strong propene chemisorption. The results reported also showed that propene is oxidized on Pt/Al_2O_3 catalysts at lower temperature than the corresponding alkane, namely propane. In this thesis, C_3H_6 combustion was used as a probe reaction to measure the influence of SO_2 aging on a DOC.

3.2.1. Kinetics and reaction parameters of propene oxidation

In order to determine the mechanism and the rate determining step of the catalytic combustion of propene, many kinetic studies have been conducted [36-39]. The Langmuir-Hinshelwood model, implying surface reaction between propylene and oxygen, is the preferred mechanism. TPD of propene and oxygen evidenced that propene adsorbed associatively on Pt/Al_2O_3 and is more strongly bound to Pt than oxygen [38]. This is in agreement with the negative partial order found for propene and the positive partial order calculated for oxygen [37, 38]. Based on these findings, it was suggested that propene is self-inhibiting by covering the platinum sites and that the dissociative adsorption of O_2 was the rate determining step of the reaction on Pt/Al_2O_3. The reported activation energy varies in the literature: 85.8 kJ/mol [38], 20-50 kJ/mol [37] and 41.9 kJ/mol [39] have been estimated.

3.2.2. Particle size effect on propene oxidation

Carballo and Wolf [39] early noted that, at low propylene concentration, the reaction rate increased with propylene concentration until a maximum. The rate then decreased with further propylene concentration increase and became propylene independent. They also measured a higher specific rate on aged catalyst which indicated a higher intrinsic activity of larger Pt particles. The global rate was, however, higher on well-dispersed catalysts. Denton et al. [17] found that the dispersion was the critical factor in the C_3H_6 combustion. They examined Pt catalysts on different supports with different porosity, impurity content and a wide range of dispersion and reported that low-dispersion catalysts of all categories were the most active for propene oxidation. In contrary, Haneda et al. [40] recently observed the decline of C_3H_6 oxidation with the dispersion loss, in agreement with Marécot et al. [41].

3.2.3. Thermal behavior during C_3H_6 oxidation

The propene combustion is exothermic with a standard enthalpy of -2058.4 kJ/mol. In a monolithic catalyst, the heat released by the reaction generates a temperature gradient that, in its turn, influences the local reaction rate. Figure 6 shows the temperature rise due to combustion light-off and the temperature gradient existing between the inlet gas and the intra-catalyst gas at 100 % C_3H_6 conversion. The propene combustion ignition has been investigated using spatially resolved technique by Epling et al. [42, 43]. It was shown during a temperature ramping that the conversion increases from front to back, at low conversion. As a consequence, a temperature rise appeared first in the monolith back. The temperature rise propagated to the upstream positions, as the 100 % conversion point shifts closer to the inlet, describing a back-to-front heat wave. For a given axial position, the temperature peaked when the conversion reached 100 % and then decreased as the ignition front moved to the inlet. At the end, only a short part of the catalyst was used to oxidize propene and an important temperature gradient developed: the front temperature, where the reaction occurs, was much higher than the back temperature. Finally, thermal aging yielded a slower back-to-front propagation of the light-off [42], whereas sulfation increased the light-off temperature but increased the speed of the ignition wave [43].

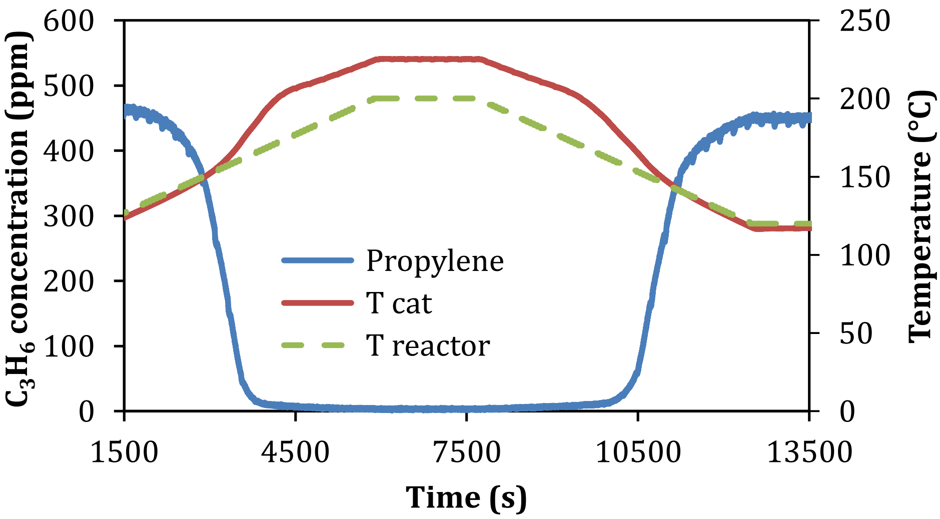

Figure 6: Temperature profiles measured at catalyst inlet (T reactor) and inside the monolith (T cat) during propylene oxidation. Propylene concentration profile showing the correlation between temperature variation and combustion light-off is also added.

3.2.4. Inhibition of C_3H_6 oxidation

Propene oxidation in presence of other components has been studied, especially for the purpose of lean NO_x reduction by HC [31, 44]. As previously mentioned, propene has a detrimental effect on NO oxidation due to its strong adsorption on Pt. This inhibition is reciprocal since the increase of the light-off temperature due to the presence of NO has been observed [30-32] and the explanation proposed invoked the occupation of active sites by NO. Propene oxidation is also self-inhibited by the strong propene adsorption and low concentration is therefore recommended to obtain a high conversion, as noted by Carballo and Wolf [39]. Haneda et al. [40] ascribed the low rate on low-dispersion catalysts to the slow reaction of formed acrylate intermediates. Thus, it was suggested that the accumulation of acrylate species on the active sites inhibited the C_3H_6 oxidation. During CO oxidation, the presence of C_3H_6 induced the building of more hindering surface intermediates, suggesting surface poisoning by C_3H_6 [45].

Chapter 4

Selective catalytic reduction of NO_x by ammonia

4.1. NH_3-SCR

The reduction of NO_x with ammonia has proved to be efficient when applied to stationary sources and does not require extra fuel to reduce NO_x, unlike NO_x storage and reduction (NSR) and hydrocarbon-SCR. On the other hand, ammonia, usually in the form of urea dissolved in solution, must be stored and carried onboard in an additional tank which is also constraining the application on passenger cars but acceptable for heavy-duty trucks.

The stoichiometry for NH_3 SCR in oxygen-containing conditions involves as much NO as NH_3 and gives N_2 and H_2O (Eq. 4.1)

$$4\ NO + 4\ NH_3 + 3\ O_2 \rightarrow 4\ N_2 + 6\ H_2O \qquad (4.1)$$

The reaction (4.1) is often referred to as "Standard SCR" and takes place when the NO content of NO_x is 100 %. Most of the NO_x released from the engine is on the form of NO. However, the DOC upstream of the SCR catalyst produces significant amount of NO_2. When a mixture of both NO and NO_2 is available, the two following reactions can occur:

$$4\ NH_3 + 2\ NO + 2\ NO_2 \rightarrow 4\ N_2 + H_2O \qquad (4.2)$$

$$4\ NH_3 + 3\ NO_2 \rightarrow 7/2\ N_2 + 6\ H_2O \qquad (4.3)$$

Reaction (4.2) is called Fast-SCR because it occurs faster than the Standard SCR and shows a maximum rate with equal amounts of NO and NO_2 [46-49]. The relative rate of the third reaction, denoted NO_2-SCR, depends on the catalyst and the conditions under which it is used. The NO_2 SCR can be faster than the Standard SCR on a Fe-zeolite catalyst [50] but slower on a vanadia-based catalyst [47]. In general, the rate of reaction of SCR increases with concentrations of O_2 and NO_x but NH_3 inhibits the reaction by blocking the active sites for NO adsorption and oxidation [50]. This inhibition is more severe on iron-containing catalysts.

4.2. Catalysts

Commercial catalysts based on vanadium oxide, like V_2O_5-WO_3/TiO_2, have been extensively studied for their excellent activity and selectivity [47, 48] for ammonia SCR. Their major drawbacks are the volatility and toxicity of vanadium oxide and a lack of efficiency at low and high temperatures. The ideal catalyst for an automotive application would cover a wide range of temperature since it is low after starting the engine (cold start) and high during the exothermic regeneration of the particulate filter, located upstream. Ion-exchanged zeolite catalysts have also been investigated extensively [46, 51-53]. Iron and copper ion-exchanged zeolites have been especially well-studied and have evidenced a good ability to reduce NO_x. The recent Cu-chabazite formulation also shows good hydrothermal and HC resistance [54-56]. Owing to their storage ability, zeolites can store unused NH_3 that can be subsequently utilized for SCR. This feature can facilitate the NH_3 dosing into the catalytic system.

4.3. Side reactions

In general, several reactions other than SCR involving either NO or NH_3 occur on the catalyst. These reactions have a detrimental impact on the selectivity and on the catalyst efficiency. NH_3 oxidation might result in over-consumption of NH_3.

At low temperature (<200°C), the main side reaction is the formation of ammonium nitrate [47, 48, 51] onto the catalyst (see reaction (4.4)). NH_4NO_3 can form a deposit on the catalyst or sublimate to exit the catalyst in the gas flow.

$$2\,NH_3 + 2\,NO_2 \rightarrow NH_4NO_3 + N_2 + H_2O \qquad (4.4)$$

The NH_4NO_3 can subsequently decompose into N_2O and water (eq. 4.5), which is suggested in many studies and is problematic since it affects directly the selectivity.

$$NH_4NO_3 \rightarrow N_2O + 2\,H_2O \qquad (4.5)$$

An alternative proposed by Koebel et al. [47] is the decomposition in NH_3 and nitric acid to oxidize NO to NO_2 which enhances the SCR reaction. In that case, ammonium nitrate is an intermediate species that builds up in presence of NO_2 and then decomposes according to the SCR reaction. The second undesirable reaction is the formation of N_2O which decreases the selectivity. One route is the direct oxidation of NH_3 according to the following reaction (4.6).

$$4\,NH_3 + 4\,O_2 \rightarrow 2\,N_2O + 6\,H_2O \qquad (4.6)$$

This reaction is the major source of N_2O over vanadia-based catalysts. Since NO_2 is a stronger oxidant than O_2, it also participates in the oxidation of NH_3. This reaction was found to be predominant over Fe-zeolite SCR catalyst by Devadas et al. [46] whereas no N_2O was formed when only NH_3 and O_2 flowed through the catalyst suggesting that the direct NH_3 oxidation (reaction (4.6)) is not responsible for N_2O production on this type of catalyst. This is also the case for Cu zeolites. At high temperature, N_2O decomposes into N_2 and O_2 and can also be reduced in parallel by NH_3 yielding an over-consumption of NH_3. With intra-catalyst measurements, Luo et al. showed that N_2O builds up in the front part of Fe/zeolite catalysts and that a fraction subsequently decomposes in the rear part of the catalyst at 500°C [50]. At low temperature N_2O generation can be explained by the decomposition of ammonium nitrate as previously mentioned (reaction (4.5)).

At high temperature, direct oxidation of ammonia is observed leading to an over-consumption of NH_3. This reaction lowers the NO_x reduction due to the competition for ammonia. It has been observed over Cu-ZSM-5 that this reaction starts above 325°C when only NH_3 and O_2 are in the gas flow [52] and the decrease of SCR observed at higher temperature can be ascribed to ammonia oxidation [52, 57]. Moreover the product of ammonia oxidation observed was N_2 [52] and not NO suggesting the following reaction equation:

$$4\,NH_3 + 3\,O_2 \rightarrow 2\,N_2 + 6\,H_2O \qquad (4.7)$$

Cu-exchanged zeolite catalysts show a high level of activity for SCR with ammonia and also limit side reactions. The NH_3 conversion and the NO conversion were found to be equal up to around 600 K, indicating a NH_3/NO stoichiometry of 1 [52, 57]. At higher temperature, NH_3 starts to be oxidized by O_2 and a too high copper content produces more N_2O.

To summarize, NO_2 enhances the NH_3 SCR but is also responsible for NH_4NO_3 formation and N_2O generation depending on the temperature. Thus, the NO_2/NO_x ratio should be well adjusted and, for optimal operation of the NO_x emission control catalytic system, it should not exceed 0.5.

Chapter 5

Catalyst synthesis and flow reactor measurements

5.1. Catalyst preparation

The catalyst synthesized and studied for diesel oxidation catalyst application was a 1 wt.% Pt/Al_2O_3, prepared by wet impregnation and freeze-drying technique. The deposition of noble metal onto alumina surface was performed by mixing an aqueous solution of Pt precursor, i.e. $Pt(NO_3)_2$, with an alumina slurry, under constant stirring. The alumina used had been calcined at 750°C in air, and the pH of the slurry was adjusted to 4 before the drop-wise addition of the Pt solution. The water used for synthesis was milliq water dispensed by a Millipore water purifier. After 1h under stirring, the obtained blend was poured in a special flask to be frozen by dipping the flask in liquid nitrogen. The flask containing the frozen catalyst was immediately mounted on a freeze-dryer apparatus in order to sublimate the water contained in the sample in solid form. At the end of the drying step, a yellow powder was collected and calcined in air at 500°C for 2h. The calcination step was carried out to decompose the nitrates originating from the precursor. The powder color turned to dark grey during this step.

Monolithic cores of cordierite were cut, calcined 2h at 600°C and impregnated with a blend of powder containing 80 wt.% of the catalyst described above and 20 wt.% of a binder to optimize the attachment of the washcoat to the channel walls. The Pt/Al_2O_3 powder was dissolved in a solution containing 50 wt.% ethanol and 50 wt.% water. The liquid-to-solid ratio is an important practical parameter since too dense slurry may clog the channels of the monolith while diluted slurry allows the deposition of a smaller amount of catalyst and requires too many dipping and drying steps. After soaking the monolith in the solution and homogeneous wetting of the monolith with the slurry, drying was carried out to evaporate water and ethanol at 90°C. Calcination of the deposited catalyst layer was then performed using a hot air gun at 600°C for 1min. The evaporation of the liquid phase was carried out thoroughly to deposit a uniformly thick layer of active phase throughout the monolith. The operation of impregnation and drying was repeated until the correct amount of washcoat was deposited on the walls of the monolith channels. The final mass of washcoat was around 20 wt.% of the total mass of the monolithic catalyst.

In paper III, the effect of support acidity on oxidation reactions and SO_2 storage was investigated and required the synthesis of $Cl\text{-}Pt/Al_2O_3$ and $SO_4\text{-}Pt/Al_2O_3$ catalysts. Both new catalysts were prepared in the same manner, by mixing a standard Pt/Al_2O_3 catalyst with a concentrated acidic solution containing Cl^- and SO_4^{2-} ions, respectively. The exchange between OH- groups from alumina and Cl^- /SO_4^{2-} anions occurred, which was depicted by the increase of the pH of the solution (Figure 7).

The chlorination of alumina is a well-known process to increase the acidity of alumina and used for instance in the alkylation and dehydration of alkanes. The usual chlorination method is based on pretreatment of the catalyst with a gas flow containing chlorine species such as tetrachloromethane (CCl_4), hydrochloric acid (HCl) and phosgene ($COCl_2$). Figure 8 represents the substitution reaction of surface hydroxyle by chlorine in HCl.

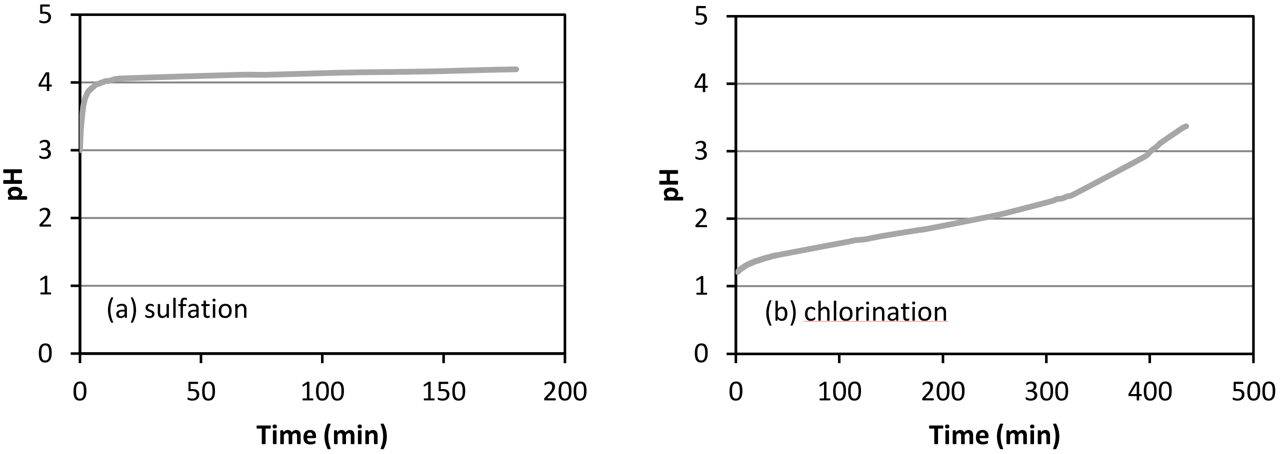

Figure 7: Evolution of the pH during preparation of sulfated (a) and chlorinated (b) Pt/Al_2O_3.

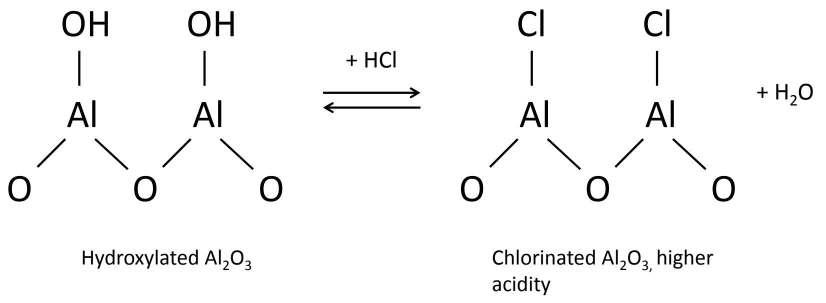

Figure 8: Mechanism of alumina chlorination by substitution of hydroxyle surface groups.

The incorporation of sulfate can be done by impregnation of the catalyst with sulfate salts like ammonium sulfate [58]. Exposition of the catalyst to a gas flow containing H_2S [59, 60] or SO_2 [61] is also widely used for catalyst sulfidation. Wet impregnation with sulfuric acid was encountered in literature [62], which was applied also in our work.

5.2. Catalyst characterization

5.2.1. BET specific surface area measurement

The samples prepared in Paper I were characterized using adsorption of probe molecules to determine their available surface area before and after aging. The surface area was measured by physisorption of N_2 at 77 K and calculated according to the Brunauer-Emmett-Teller Theory (BET). This measurement gives a value representing the physical surface area of the catalyst without differentiating between surfaces of different chemical properties, like metal particle and metal oxide support. An automatic instrument Micromeritics ASAP2010 was used for this measurement. The measurements were carried out on the coated monoliths after drying in vacuum for 2 h at 225°C.

5.2.2. Platinum dispersion measurement

CO chemisorption experiment was performed in the flow reactor described in section 5.2.4 in order to estimate the platinum dispersion, i.e. the fraction of platinum particle surface exposed. A 20 min pulse of gas containing 100 ppm of CO was first sent over the catalyst where CO adsorbed. A flow of pure argon was then fed to remove weakly bound CO and a second pulse similar to the first one was conducted for 10 min. During the whole experiment, the total flow was 1L/min and the carrier gas was Ar. The uptake of CO was measured for the two steps. The chemisorbed CO was then calculated by subtracting the physisorbed CO and the reactor system contribution, measured in the second CO pulse. The number of surface Pt atoms was inferred assuming that CO adsorbed on the surface with the ratio CO:Pt= 0.8 according to the results of Foger et al [63] and Olsson et al. [33] (Figure 9). The expression for the dispersion was then:

$$D_{Pt} = \frac{Pt_{exposed}}{Pt_{total}} = \frac{CO_{chemisorbed}}{N_A * m_{cat} * loading * 0.8}$$

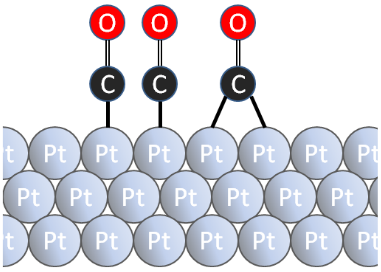

Figure 9: Schema of CO adsorption on Pt particle surface for measuring the dispersion.

Dispersion and average particle size are correlated and different relations have been proposed assuming different particle shapes. Assuming spherical particles (or hemispherical with the flat surface in contact with the support) Guo et al. proposed the relation $d_{Pt} = \frac{1{,}07}{D_{Pt}}$ where d_{Pt} is the average particle size and D_{Pt} is the platinum dispersion [64]. The CO:Pt ratio was kept constant for all the analyzed data, assuming that the stoichiometry of CO chemisorption does not depend on particle size. This simplification is not fundamentally correct since the stoichiometry of CO adsorption on Pt varies between 0.6 and 1 [65].

5.2.3. Transmission electron microscopy

Transmission electron microscopy was used in Paper I to characterize the fresh and SO_2 aged catalysts and to support the dispersion results calculated from CO chemisorption. The catalysts powders were ground in an agate mortar and subsequently put on holey carbon films on TEM Cu grids. The particles were imaged using an FEI Titan 80-300 TEM with a probe Cs (spherical aberration) corrector operated at 300 kV. The images were recorded using a high angle annular dark field (HAADF) detector in the scanning TEM imaging mode (STEM), providing Z number contrast. The electron probe size was about 0.2 nm for these studies. Figure 10 shows a STEM micrograph of the fresh catalyst. The synthesized catalysts are well-dispersed with a low average particle size (≈1nm).

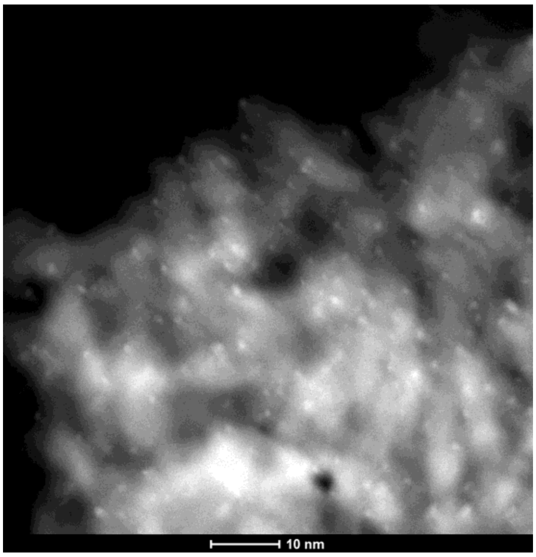

Figure 10: STEM micrograph of the fresh 1wt% Pt/Al_2O_3 catalyst.

5.2.4. Reactor setup

All experiments (aging, dispersion measurement and activity test) were performed in similar flow reactors composed of a quartz tube heated by a coiled electric resistance (DOC studies) or a furnace (SCR study) in which the monolithic catalyst was placed. The reactors were equipped with a set of mass flow controllers that supplied gases with the appropriate volumetric flow. The outlet of the reactors was connected to analysis instruments in order to measure and record the effluent gas chemical composition. In paper I, specific detectors were mounted on the reactor to detect CO, CO_2, NO and NO_2. The reactor used to perform the other DOC studies was equipped with a mass spectrometer and a gas FTIR analyzer that could simultaneously detect quantitatively various gases. For the intra-catalyst study of NH_3-SCR, one MS was used.

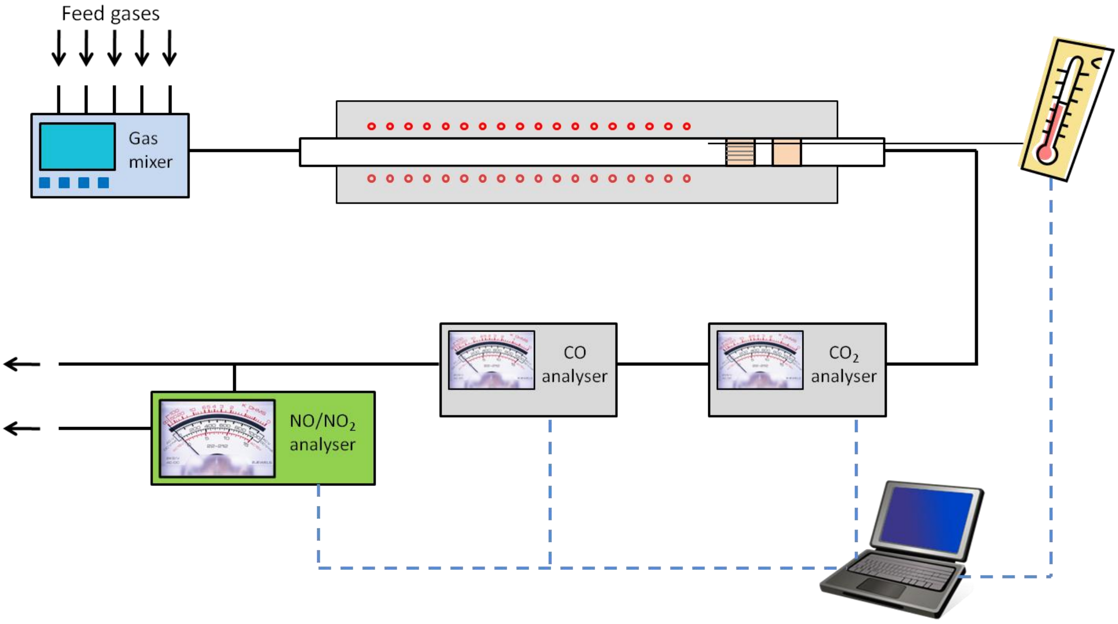

Figure 11: Schematic representation of the reactor setup used in Paper I.

5.2.5. Temperature control

In all experiments, thermocouples were inserted from the back of the reactor. The number of thermocouples used varied with the reactor employed. In general, one thermocouple was placed in front of the catalyst and controlled the heating system to make the temperature equal to the set temperature at that position. A second thermocouple was placed in a channel of the monolith in order to measure the catalyst temperature. Efforts were made in order to reproduce the probed position (chosen channel and depth into this channel). An additional thermocouple and an empty monolith were placed downstream in Paper I, to limit and check the temperature gradient.

5.2.6. NO oxidation

NO oxidation activity was measured on degreened and aged catalysts using the following procedure. A flow of 3000ml/min containing 500 ppm NO and 8 % O_2 with or without water vapor (5 %) was sent over the catalyst for 30 min at room temperature in order to saturate the surface with NO. Then the temperature was ramped up to 500°C at the rate of 5°C/min. The NO and NO_2 concentrations of the outlet gas was quantified by a chemiluminescence NO_x analyzer and recorded at the frequency of 1Hz, in Paper I. In Paper II and III, multigas FTIR was employed to record quantitatively the NO_x outlet concentrations.

After the ramping, the temperature was held constant for 5 min at 500°C to make sure that steady state was established. The same gas flow was maintained during the cooling. In Paper II and III, the cooling was operated at the same controlled rate as the heating in order to measure the activity during extinction and characterize the hysteresis behavior of the reaction.

5.2.7. C_3H_6 oxidation

C_3H_6 oxidation activity was evaluated in flow reactor by similar temperature-programmed reaction in presence of 5 % H_2O. The temperature was increased and then decreased at a rate of 1°C/min between 130°C and 250°C. Propene outlet concentration was measured by the FTIR instrument.

5.2.8. Aging under reactive atmosphere

The aging procedure was the same for each catalyst and all aging temperatures, and was performed in the flow reactor used for the activity test. Initially an Ar flow of 1000 mL/min was sent over the catalyst for 10min at room temperature before starting to heat the reactor up to the aging temperature. As soon as the reactor temperature stabilized at the target temperature the catalyst was exposed to its reactive atmosphere for 2h. After this period, the aging atmosphere was replaced by a flow of pure Ar and the reactor was cooled. The total flow remained constant during the entire process (1000 ml/min) and only the gas composition varied from pure Ar to aging atmosphere. Like the heating, the cooling was as short as possible. To accelerate the cooling step, the insulation wool around the reactor was immediately removed after the 2h aging step.

5.2.9. Advanced analytic technique: SpaciMS

In automotive catalysis, monolithic converters are used in order to achieve a high gas-catalyst interface and a low pressure drop. Ideally, a monolith behaves like a plug-flow reactor and concentrations of reactants and products evolve along the catalyst. These intra-catalyst evolutions cannot be detected with the usual flow reactor experiments and analytical techniques. It is of importance to know what occurs inside the catalyst in order to assess the reaction mechanisms. For example, reaction intermediates can be formed at the front of the catalyst and subsequently react. Intra-catalyst measurement is a large advantage in order to investigate these features.

For this purpose the Spatially Resolved Capillary Inlet technique has been developed and was first adapted to mass spectrometer by the Oak Ridge National Laboratory and Cummins Inc. [4, 66-69] and was later also used together with FTIR spectrometer [50]. A flexible capillary is connected to the instrument inlet and the other end is inserted into a selected channel of the monolith (Figure 12). The capillary is typically made of fused-silica and coated with polyimide; its outer diameter is ca. 150-200 µm. The capillary tip can be translated throughout the catalyst in order to determine the gas composition at any position. Such data are valuable for the development of kinetic models since it allows one to collect data at realistic flow rate and temperature leading to high, if not full, conversion at the catalyst outlet.

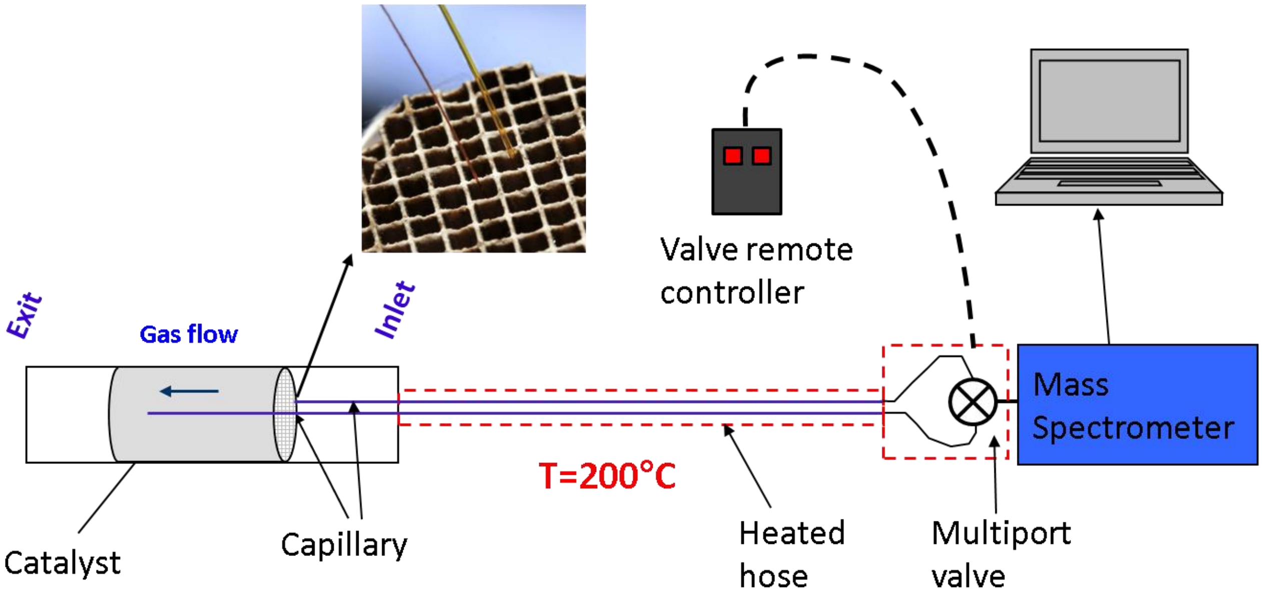

Figure 12: Schematic representation of SpaciMS system.

One difficulty with intra-catalyst measurement is the flow disturbances caused by the capillary. This effect depends on the volume of the capillary actually present in the catalyst. Thus, the outer diameter of the capillary is an important parameter. It should be much less than the channel diameter to limit the impact on the gas flow. The capillary probe pumps reaction gases, which modifies locally the concentrations of the reactants, the pressure and the flow velocity. A low sampling rate of ca. 10 µL/min limits this effect. Sà et al. [70] have investigated the intra-catalyst oscillations of the concentrations and temperature for the oxidation of CO. Using measurements and CFD simulations, they demonstrated that the intrusion of a capillary probe in a channel had a negligible effect on the catalyst behavior. Another drawback of using a capillary inlet is the interactions between gas molecules and the inner surface of the capillary. They become non-negligible as the inner diameter of the capillary decreases and when the flow is decreasing. Interactions are greater for sticky molecules, such as NH_3 and NO_2. This can cause that the instrument response to a pulse is a more or less broad peak which complicates the time resolved analysis. The capillary was heated and maintained at 200°C to weaken molecular interactions with the capillary walls and reduce adsorption inside the capillary. In this way, the time resolution was improved.

SpaciMS has been successfully used at ORNL for investigating lean NO_x-trap catalyst behavior during storage and regeneration [66-68] and fuel cells [69]. Other groups have performed intra-catalyst measurements on various reactions to get an insight into the spatial consumption of reactants [42, 50, 71, 72].

For the second part of this thesis, the SpaciMS technique has been adapted to study the reduction of NO by NH_3 according to the NH_3-SCR reaction. These experiments were conducted at Oak Ridge National Laboratory in USA.

5.2.10. Reactor setup

The micro reactor used for the NH_3-SCR study is shown in Figure 13. It was composed of two cylindrical furnaces. The larger one was the pre-heater, in which feed gases circulated into coiled pipes to be heated up before subsequent mixing. The furnace with smaller diameter contained the quartz-tube reactor into which the catalyst was placed. Quartz rods were placed in the tube upstream and downstream from the catalyst to create gas mixing and to lower the axial temperature gradients inside the reactor.

The capillary probes were inserted into the tube from the inlet (right side of the reactor on Figure 13) and K-type thermocouples were inserted from the outlet. The gas flows were metered by mass flow controllers and sent to two three-way switching valves, which were computer controlled. These electrovalves enable a fast turnaround time when switching gas stream to the reactor. The gas lines between the pre-heater and the reactor, at the outlet of the reactor as well as the capillaries were heated and maintained at a temperature above 200°C to avoid adsorption in the pipes and the formation of ammonium nitrate. Two capillary probes, the tips of which were separated by 1.25 inches, were actually used during all experiments. One capillary was placed into the catalyst, while the second was always located in front of the catalyst. Both capillaries were connected to a multiport valve, connected to the MS inlet. The gas flow from either of the capillaries could be selected for analysis and switching from one capillary to the other was made during experiment with a remote control (Figure 12). The inlet gas composition was determined at the end of each step, by switching to the inlet capillary, to get a better contrast between inlet and intra-catalyst concentrations.

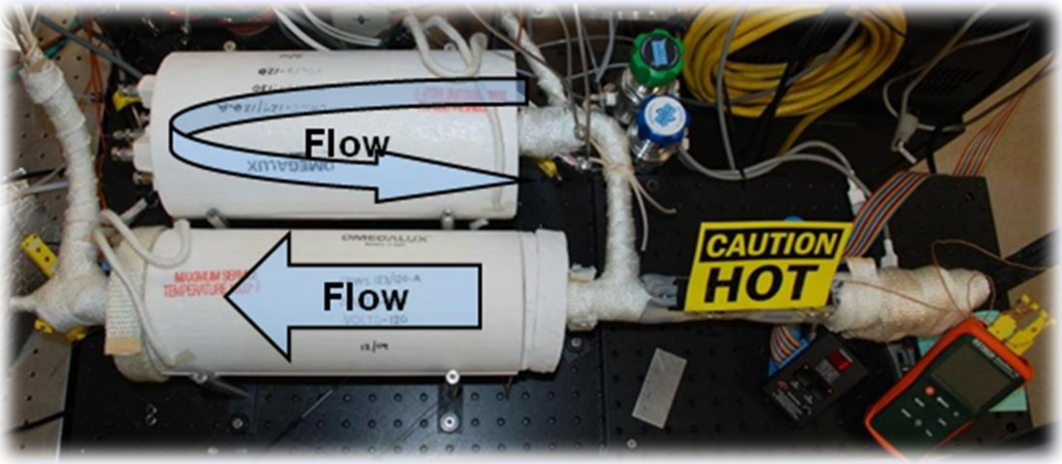

Figure 13: Picture of the reactor setup for the spatio-temporal study of NH_3-SCR at Oak Ridge National Laboratory.

Chapter 6

Challenges specific to automotive catalysts: aging and sulfur poisoning

Catalysts often lose their activity with operating time and need to be replaced or regenerated. In automotive emission control catalysis, this deactivation is mainly caused by durable catalyst poisoning and sintering. The sintering is the loss of catalytic surface due to collapse of the pore structure and metal agglomeration. These phenomena take place at elevated temperature. The poisoning is the alteration of the catalyst caused by a chemical component that reacts with or blocks the active sites.

6.1. Aging of catalyst

6.1.1. Thermal aging

When a supported catalyst is subjected to high temperature, structural changes occur. The porous support can lose surface area by pore collapse leading to the formation of larger pores. Phase transition can also affect the surface area of the support material. Thus, loose packed γ-Al_2O_3 is converted to close packed α-Al_2O_3, the stable form of alumina, at high temperature. The temperature increases also the mobility of the metal nanoparticles on the surface, which consequently start to migrate. This phenomenon results in metal agglomeration in larger particles, more thermodynamically stable due to a lower fraction of low-coordinated atoms. This process is called sintering and generally causes a loss of activity correlated to the loss of exposed surface sites. Figure 14 illustrates the decrease of Pt dispersion owing to aging at high temperature (600, 700, 800 and 900°C) in an inert gas flow. A linear dispersion decrease can be noted until 700°C, followed by a plateau at higher temperature. The mechanism and the kinetic of sintering have been studied to develop a sintering model. Two models were proposed: the particle migration model [73] and the atomic migration model [74, 75]. In the former, Ruckenstein and Pulvermacher described the formation of large particles by migration of small particles on the surface and their incorporation to the larger particles structure by collision. This model implies the decrease of the total number of particles. Flynn and Wanke [74, 75] suggested that sintering was initiated by extraction of metal atoms or molecules from small particles followed by the rapid transport of these free atoms to large particles. This mechanism, also known as Oswald ripening, predicts simultaneous shrinkage of small particles and growth of larger particles. It can also explain the redispersion of sintered catalysts by a rapid cooling, early in the sintering process, when atoms accumulate on the surface or the presence of trapping sites on the support that are able to anchor the free atoms during their migration. The driving force of Flynn and Wanke's model is the particle size difference which implies no sintering of unisized catalyst and faster sintering for a catalyst presenting a broad particle size distribution. Experiments have showed that a mixture of fresh and presintered catalyst, i.e. containing large particles, sinters more rapidly [76].

In Paper I, aging in argon showed to decrease the platinum dispersion linearly until 700°C (Figure 14). After further aging at higher temperature, only minor dispersion loss was observed and the dispersion leveled off.

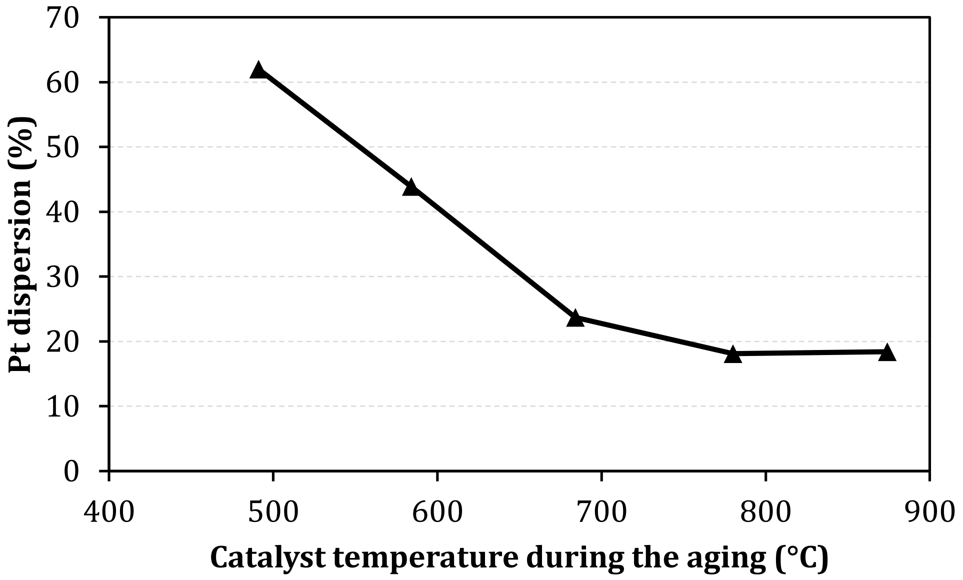

Figure 14: Pt dispersion decrease by thermal aging (2h at 600, 700, 800 and 900°C) in argon flow.

The activity resulting from the dispersion changes are presented in Figure 15, where the activity improvement by each aging step is evidenced. These results show that large particles are more active for NO oxidation, in agreement with several studies in literature [6, 12, 15, 17].

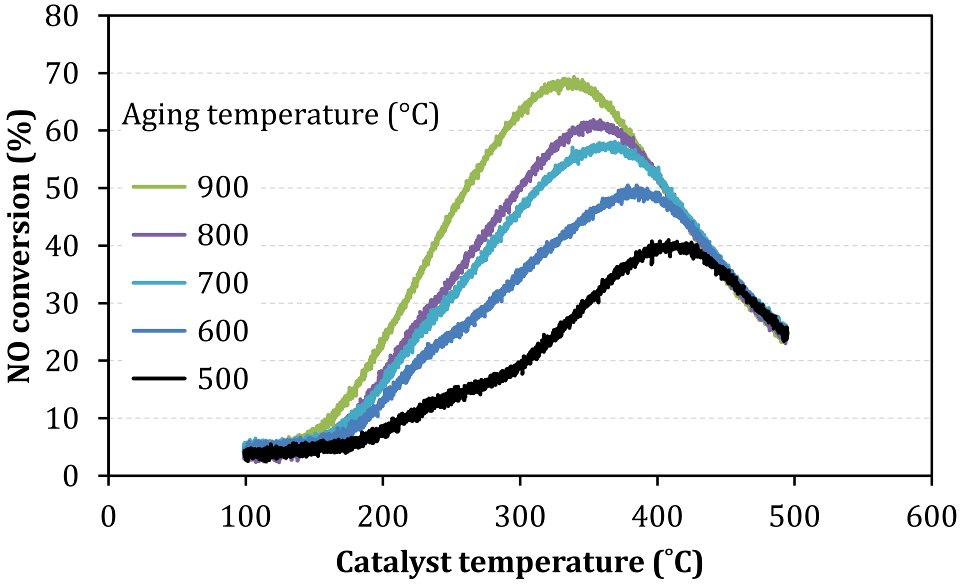

Figure 15: NO oxidation activity of Pt/Al_2O_3 degreened (labeled as 500) and aged at 600, 700, 800 and 900°C. Gas composition: 500ppm NO + 8% O_2 in Ar (3L/min); ramping rate 5°C/min.

6.1.2. Effect of reactive atmosphere

The objective in Paper I was to investigate the role of different aging atmosphere on the dispersion evolution. Indeed, the atmosphere has a significant role in the sintering rate since it can influence the support-metal interaction and yields the formation of intermediate species, such as PtO_x in the case of aging in oxygen, that enhance the Pt atom mobility. Figure 16 reports the dispersion of catalysts aged in different atmospheres after each aging step.

Effect of O_2

In presence of oxygen, the dispersion decreases linearly with aging temperature, as for argon aging. However, the minimum dispersion attained after aging at 900°C was lower in presence of O_2. Oxygen can form platinum oxides molecules that migrate from the particles according to the atomic migration mechanism [77]. This process is able to explain the redispersion observed in presence of oxygen [78] at temperature below 600°C. Above this temperature, Pt oxides decompose to metallic platinum and oxygen. Lee and Kim [78] suggested that Pt atoms formed on the surface were likely very mobile and would be captured by large particles. At high temperature, Pt can be transported in vapor phase as $PtO_{2(g)}$ and deposited on the surface where the oxide decomposes. Matam et al. [20] noted the more pronounced decrease of dispersion, measured by CO chemisorption, of a model DOC aged in oxidative atmosphere compared to lean diesel exhausts atmosphere, containing also CO and HC. They also observed that aging in air led to heterogeneous particle size and the formation of very large particles.

Effect of H_2

In H_2, the dispersion decreased only moderately at 600°C indicating a slower sintering process. After aging at 700°C, the catalyst aged in H_2 still had the highest dispersion but presented, after the last aging step, similar dispersion as the argon catalyst.

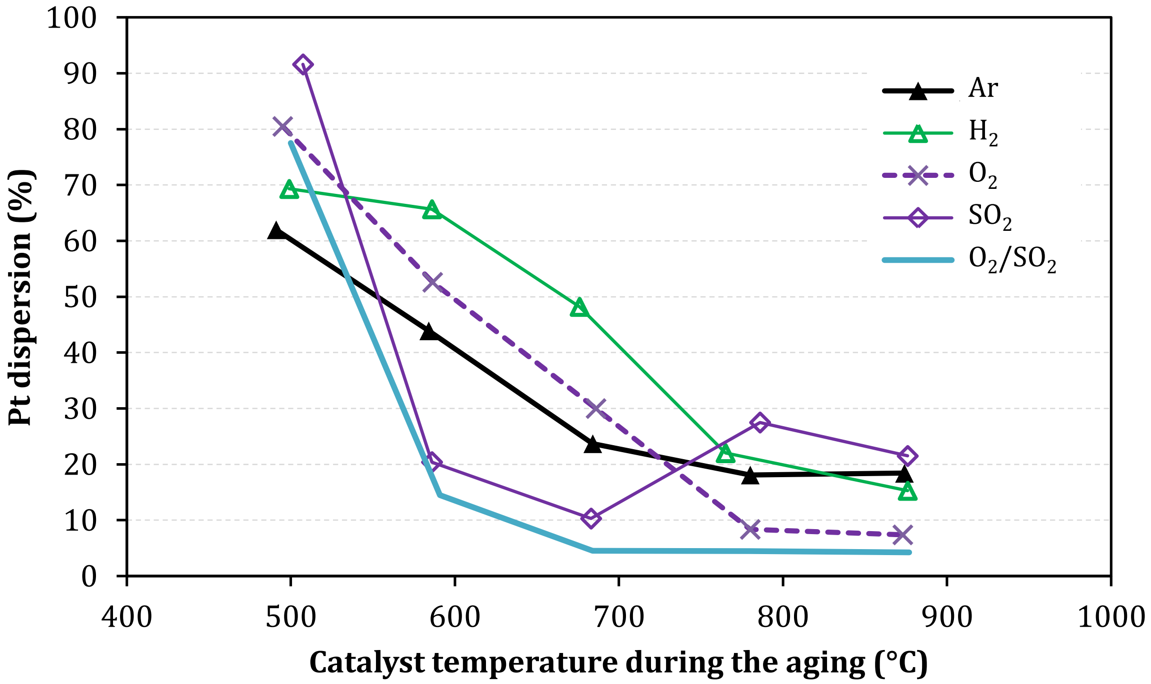

Figure 16: Evolution of Pt dispersion with aging temperature of catalysts aged in different atmospheres (Ar, 10% O_2, 1% H_2, 30ppm SO_2 and 30ppm SO_2 + 10% O_2).

Effect of SO_2

Figure 16 shows that the presence of SO_2 during aging led to significant dispersion drop already at 600°C. However, the apparent Pt dispersion increased after aging at 800°C in 30 ppm SO_2 which could be the result of either Pt redispersion, promoted by SO_2, or underestimation of dispersion by CO chemisorption after aging at 600 and 700°C. The reduction treatment prior to dispersion measurement can reduce SO_2 species to atomic S, which covers the platinum particles and decreases the available platinum surface. The redispersion feature has been reproduced on a second sample aged in SO_2, but attempt to redisperse aged catalysts by SO_2 treatment at 800°C failed. It is possible that the dispersion after SO_2 aging at temperature lower than 800°C was underestimated. The important sintering at the end of the procedure was however confirmed by microscopy analysis. Figure 17 evidenced the sintering with the presence of large particles homogeneously dispersed on the surface (Figure 17a) having similar size (15-20nm) and faceted morphology (Figure 17b). Chang et al. [79] investigated sulfur poisoning of Pt/Al_2O_3 catalysts and observed by EXAFS an important Pt sintering caused by sulfur. Olsson and Karlsson [80] observed a significant decrease of Pt dispersion upon SO_2 exposure, accompanied with a continuous NO conversion increase during SO_2 exposure. However, Kärkkäinen et al. [81] did not find any sintering evidence by SO_2 treatment of a Pt/Al_2O_3 catalyst.

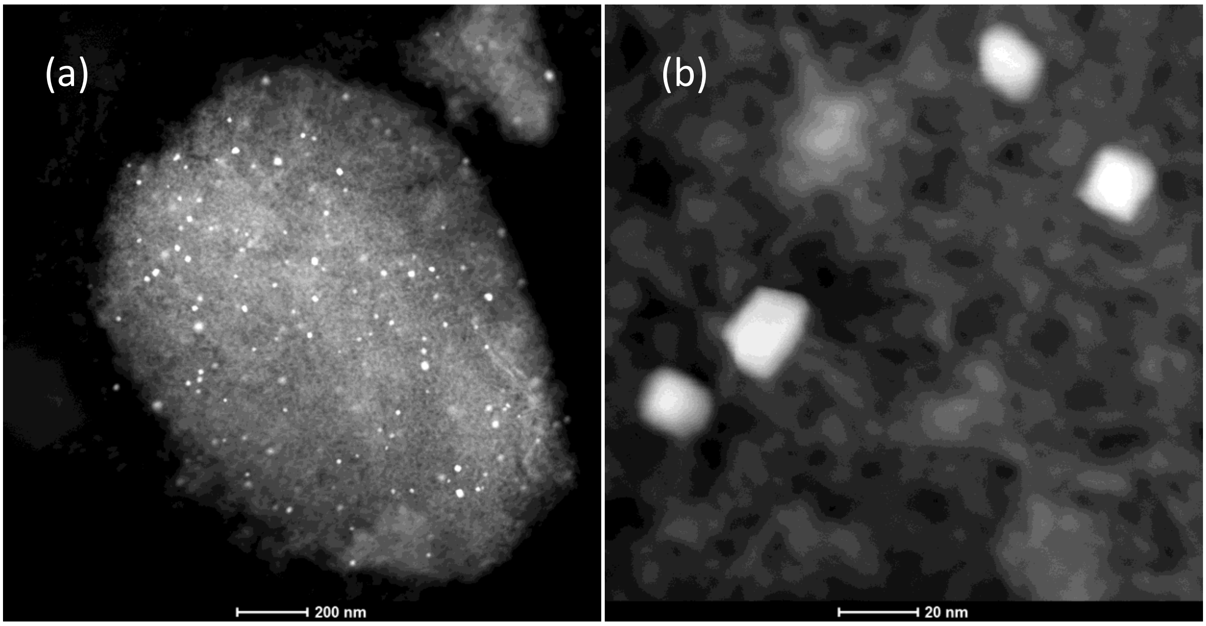

Figure 17: STEM images of Pt/Al_2O_3 aged in $SO_2 + O_2$ at the end of the aging procedure (last aging step at 900°C).

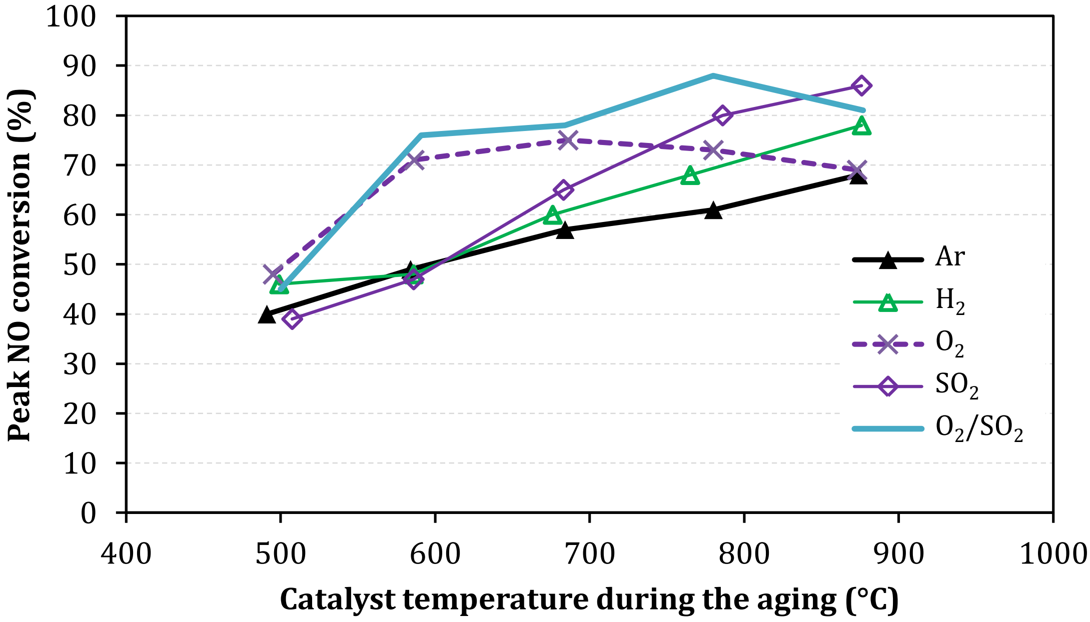

Figure 18: Evolution of catalytic activity, represented by the maximum of NO conversion reached, of Pt/Al_2O_3 catalysts aged in different atmospheres (Ar, 10% O_2, 1% H_2, 30ppm SO_2 and 30ppm SO_2 + 10% O_2).

Figure 18 represents the highest NO conversion of the catalysts after every aging steps. In general, NO oxidation activity was improved by thermal aging, as large particles demonstrated higher activity than small ones. Differences arose from aging atmosphere though. The activity of the two samples aged in presence of oxygen increased dramatically after the first aging (>70 % conversion) whereas the three other samples were moderately improved (<50 % conversion). The second particularity of the oxygen aged catalysts is the activity decline after aging at high temperature, which takes place at 800°C in O_2 and at 900°C in O_2+SO_2. The catalysts aged in Ar, H_2 and SO_2 were improved by each aging step.

The relation between activity and Pt dispersion is not straightforward indicating atmosphere-induced effects on the Pt particles. Cabié et al. [82] investigated with environmental TEM the morphology changes of Pt particles induced by the nature of the gas surrounding the nanoparticles. They evidenced the facet transition from (111), more stable under H_2 pressure, to (001) in presence of O_2.

From our aging results, it could be noticed that the catalysts aged in SO_2 and SO_2+O_2 showed the greatest activity (>80 % NO conversion), which suggested a beneficial effect of SO_2 aging and directed the continued research work in that direction.

6.2. Interaction of sulfur compounds with oxidation catalysts

SO_2 enters into the vehicle exhausts due to the presence of sulfur in the fuel as well as in the lube oil. Sulfur dioxide has a great ability to adsorb and store as sulfite or sulfate on a metal oxide material such as alumina. Alkaline sulfates, such as barium sulfates, are easily formed which results in that SO_2 is a difficult poison for Lean NO_x-trap Ba-based catalysts. This NO_x-removal technology aims at trapping NO_x by formation of barium nitrate prior their reduction into N_2. The storage of sulfur on barium sites reduces dramatically the NO_x-storage capacity.

However, SO_2 has shown interesting properties in promotion of diverse reactions. The promotion of propane oxidation [36, 61, 83, 84] and methane oxidation [85] by SO_2 has been reported.

6.2.1. Adsorption and storage of sulfur species

SO_2 adsorption and storage on catalysts has been studied by infra-red absorption and temperature-programmed reduction (TPR). Yao et al. [36] identified the formation of sulfites formed on alumina, which were subsequently oxidized into sulfates upon SO_2 exposure. SO_2 oxidation and consequently SO_2 storage is facilitated by the presence of Pt [23, 36, 86]. In absence of O_2, Corro et al. [61] observed the adsorption of SO_2 below 250°C, which was accompanied by a second SO_2 uptake at higher temperature in presence of O_2 forming sulfate species. This second uptake was greater and took place at lower temperature on Pt/Al_2O_3 than on Al_2O_3, indicating the promotion of Pt on SO_2 storage. SO_2 adsorption is also promoted by the presence of NO, both in pre-adsorbed and gas form [87]. Two main species form on alumina: sulfate, favored at high exposure temperature and long exposure time, and weakly chemisorbed SO_2. The SO_2 storage decreases at higher deposition temperature but the sulfate amount is not affected. The exposure temperature has therefore a major effect on the adsorbed species nature and stability. Wakita et al. [88] observed by XPS the simultaneous presence of sulfur as both SO_4^{2-} and S^{2-} upon exposure of catalysts to SO_2 or H_2S. They concluded that sulfate was stored on alumina and S^{2-} covered Pt. Kröcher et al. [23] suggested that sulfation in presence of water processes via oxidation of SO_2 into SO_3 and formation of liquid sulfuric acid on the surface. In a slower step, subsequent sulfation of the washcoat by stable species occurred by sulfur migration, independently of SO_2 concentration.

The support plays a crucial role in SO_2 storage since it has been observed that SiO_2, unlike Al_2O_3, was unable to store SO_2 [89]. SO_2 storage is also very low on TiO_2 support [34]. In contrary, the presence of absorbent elements such as barium boosts the sulfur storage [90]. According to the results by Streber et al. [91], on Pt (111) single crystal surface, SO_2 adsorbs molecularly at low temperature (120 K). A part of SO_2 is converted to SO_3 on oxygen precovered surface. On the clean Pt surface, slow heating creates SO_2 transition from up-standing to lying formation before all SO_2 is desorbed at 360 K. A small amount of atomic S produced by SO_2 disproportionation remains at that temperature. On O-precovered surface, heating causes the increasing SO_3 coverage at the expense of SO_2. SO_3 is subsequently oxidized in SO_4. The SO_x species starts desorbing at 230 K until the surface becomes sulfur-free at 520 K. Adsorption and thermal evolution of SO_2 on Pt(110) [92] also showed the SO_2 molecular adsorption at low temperature and the conversion to SO_3 and atomic S and subsequently SO_4. After heating to 650 K, SO_4 has desorbed and S has almost completely left the surface. This temperature suggests that in our experiments the platinum is sulfur-free after the reduction at 450°C preceding the dispersion measurement.

6.2.2. Stability of sulfur adsorbates

The IR absorption bands attributed to sulfates by Yao et al. [36] disappeared at 800°C in vacuum or 700°C in H_2 flow, indicating the high stability of these adsorbates. It has been reported that SO_2 adsorbs weakly on the basic sites and strongly on the acidic sites of alumina. The adsorption of weakly adsorbed SO_2 is increased by the presence of O_2, likely by creating new basic sites and their release takes place below 600°C [87]. However, the presence of both NO and O_2 converts weakly adsorbed species into strongly adsorbed SO_2, likely Al-O-SO_3 or SO_4^{2-}. Nam and Gavalas [93] have identified two kinds of SO_2 adsorbed species on γ-Al_2O_3 that differ in stability and reduction products distribution. The more weakly adsorbed type desorbs without reduction as SO_2 while the most stable species desorbs only during reduction as H_2S. This finding is in agreement with our results showing a category of species that decomposes into SO_2 and H_2S upon reduction at 500°C (Figure 19) and a second type of more stable species, reduced at higher temperature and producing solely H_2S (Figure 20). Figure 19 displays the SO_2 and H_2S release observed during reduction at 500°C of SO_2-aged Pt/Al_2O_3. Before the introduction of H_2 thermal desorption of SO_2 weakly adsorbed can be noticed. Introduction of H_2 immediately provokes an intense SO_2 release followed by the H_2S desorption, as observed by Nam and Gavalas [93].

Luo et al. [94] showed that sulfur release off a DOC was the most effective in presence of H_2, compared to CO, CO_2, H_2O and inert He. In contrary, oxidizing conditions inhibited sulfur release. The relative H_2S/SO_2 ratio during release of sulfur was found to be dependent on the initial sulfur loading with a higher SO_2 proportion released at high sulfur loading [94]. In reductive atmosphere, the DOC desulfation was achieved at 700°C. In the same study, Luo et al. proposed that desulfation takes place on Pt and is therefore controlled by surface sulfates migration to Pt particles.

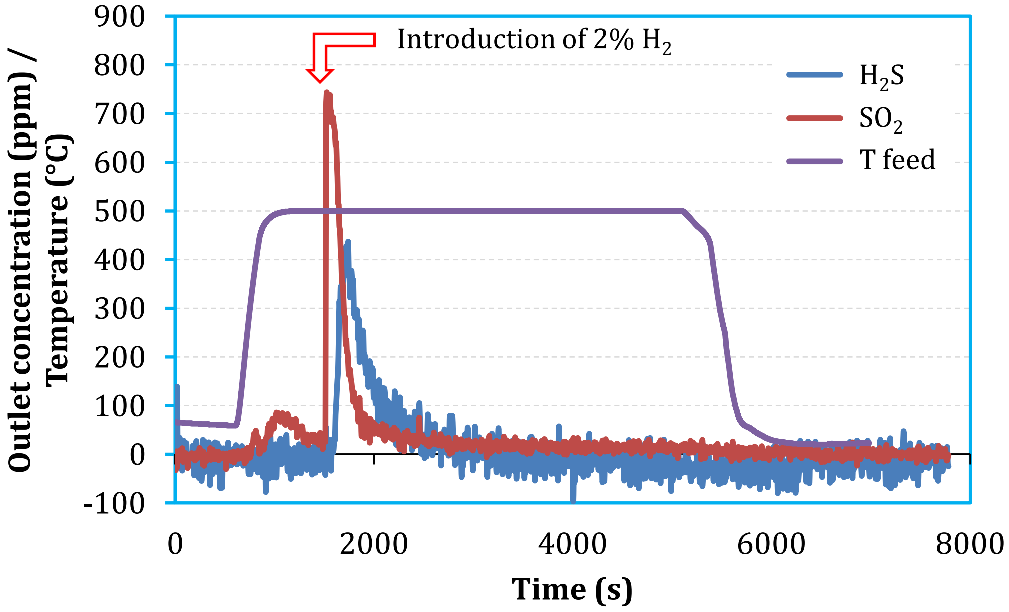

Figure 19: Species released by reduction (2% H_2) at 500°C of Pt/Al_2O_3 after SO_2 exposure.

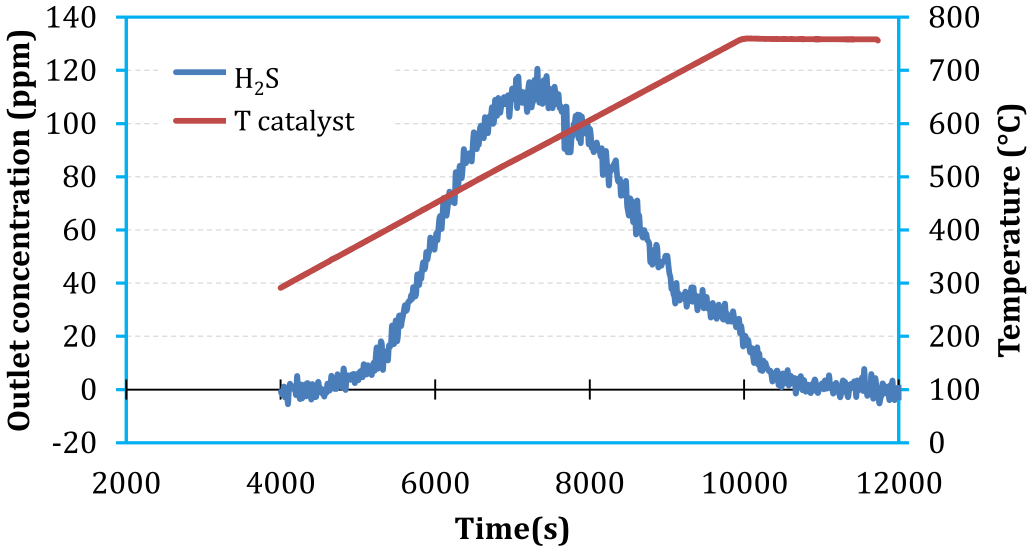

Figure 20: H_2S release during TPR of a sulfated Pt/Al_2O_3 (2% H_2, 5°C/min).

6.2.3. Interaction of surface sulfur species with a DOC in operating conditions

Many studies have revealed a promotional effect of SO_2 in combustion of saturated HC such as propane [36, 61, 83, 84]. In contrary, SO_2 reduces the activity of Pt/Al_2O_3 catalysts for CO oxidation as well as propylene oxidation [36, 43]. Li et al. [95] demonstrated that freshly deposited sulfur has a detrimental effect on NO and C_3H_6 oxidation due to its location close to the active sites, supported by a change in activation energy. On the other hand, they showed that vehicle-aged high sulfur loading catalysts presented similar activity before and after desulfation. Further experiment consisting in sulfation followed by a long step at 400°C showed that sulfur migrated from active sites to the support resulting in a minor impact on the subsequent activity, as sulfur deposited on vehicle-aged catalysts. Pazmiño et al. [96] evidenced by EXAFS the migration of sulfur from Pt particles to the support during NO oxidation conditions and concluded that the formation of nitrates could displace sulfur from Pt. Our results are in line with the sulfur migration from Pt sites to the support. They also support the conclusion of Li et al. [95] since we evidenced the major detrimental impact of the less stable sulfur species, presumably located on the Pt or the Pt-support interface, while the more stable species caused a minor activity loss for NO and C_3H_6 oxidation.

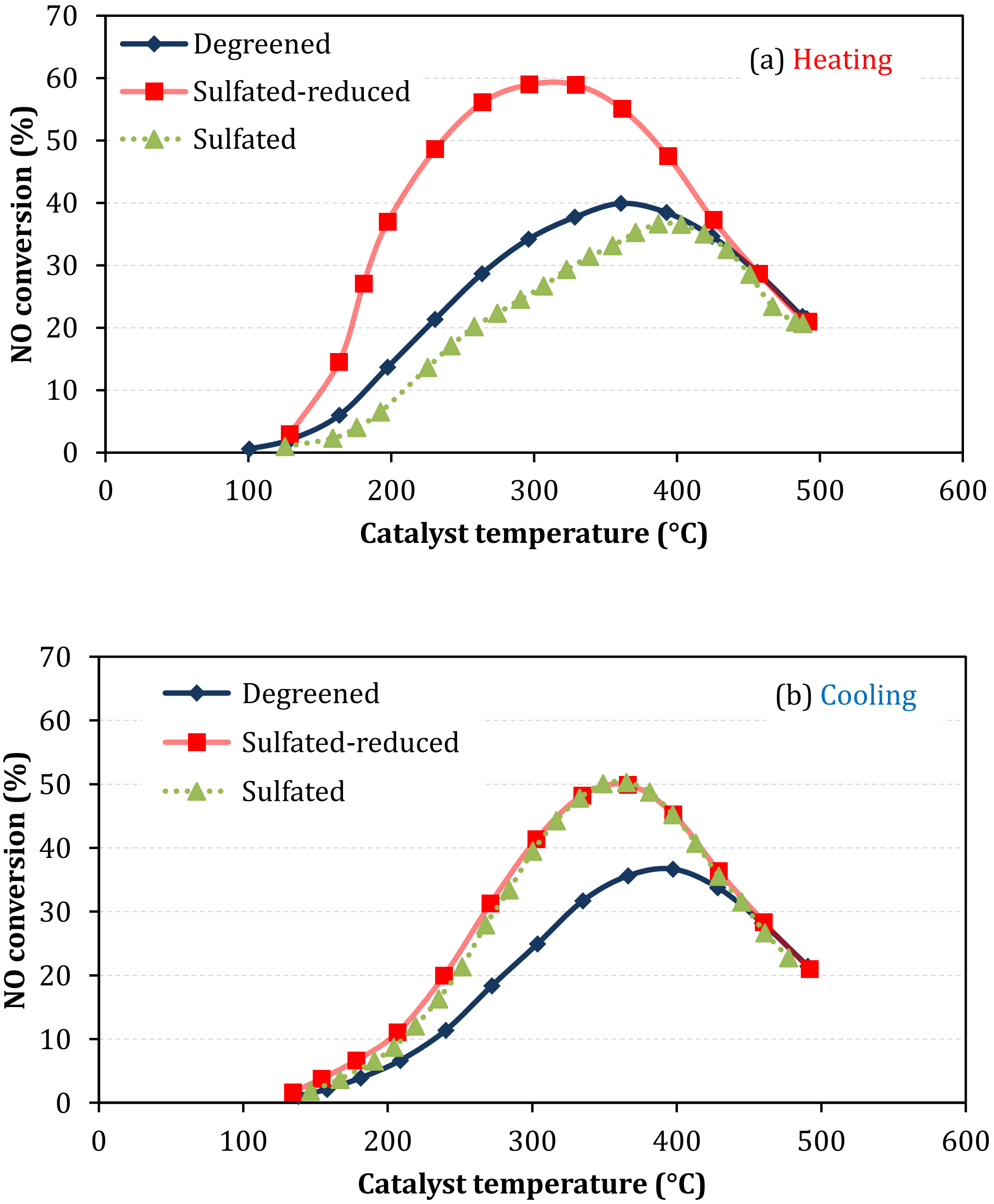

Figure 21: NO conversion measured by temperature-programmed reaction (500ppm NO + 8% O_2 + 5% H_2O) over Pt/Al_2O_3 degreened, sulfated (22h; 250°C; 30ppm SO_2 + 8% O_2 + 500ppm NO + 5% H_2O) and reduced after sulfation (1h; 500°C; 2% H_2). (a) Heating 5°C/min. (b) Cooling -5°C/min.

In Paper III, SO_2 exposure of a model DOC was conducted for 22h at 250°C in presence of water, oxygen and nitric oxide. As shown in Figure 19 and Figure 20, this treatment leads to catalyst sulfation by creation of two types of sulfur species.

Figure 21 shows the impact of sulfur species that can be released under reducing condition at 500°C on NO oxidation activity. The comparison between the activity of the degreened and the sulfated catalyst during heating shown in Figure 21a demonstrates the negative effect of this type of species. This is confirmed by the significant improvement observed after reduction and release of these sulfur adsorbates. During cooling (Figure 21b), the sulfated catalyst gained activity to display the same profile as the reduced catalyst. This observation combined with the absence of sulfur desorption during the activity tests suggests that the sulfur species have been displaced from active sites to the support and therefore had a minor effect during the cooling.

The SO_2 exposure effect is worth to mention since a tremendous activity increase was noted after sulfation and reduction. However, if the samples were not reduced after the sulfation, it had a negative effect on C_3H_6 combustion, characterized by an increase of 50 % conversion temperature (T_{50}) of 12°C. The same effect of DOC sulfation was reported by Russell et al. [43]. Since C_3H_6 oxidation test directly followed the NO oxidation step in our protocol, the lower C_3H_6 oxidation performance, during heating (Figure 22a), due to sulfation indicates that sulfur migrated back to the active sites after having been displaced by NO at high temperature as observed by Pazmiño et al. [96]. However, this sulfur migration did not occur in the presence of propylene as suggested by the absence of activity recovery during cooling (Figure 22b). The reason can be the lower temperature applied in the C_3H_6 oxidation experiment or the weaker competition of C_3H_6 for adsorption sites. The reduction of sulfated sample, however, revealed the beneficial effect of SO_2 exposure on C_3H_6 combustion since higher activity was measured after the treatment for both heating and cooling.

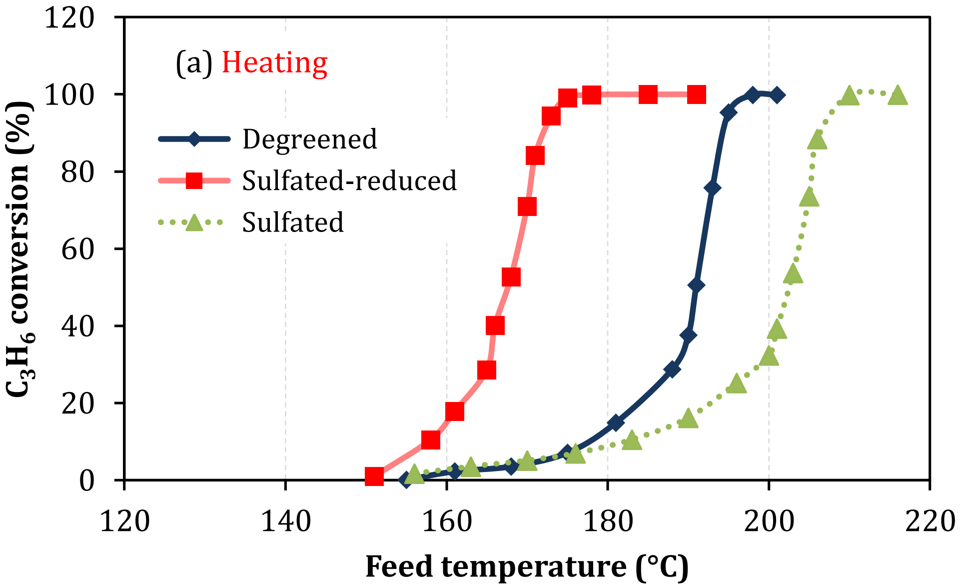

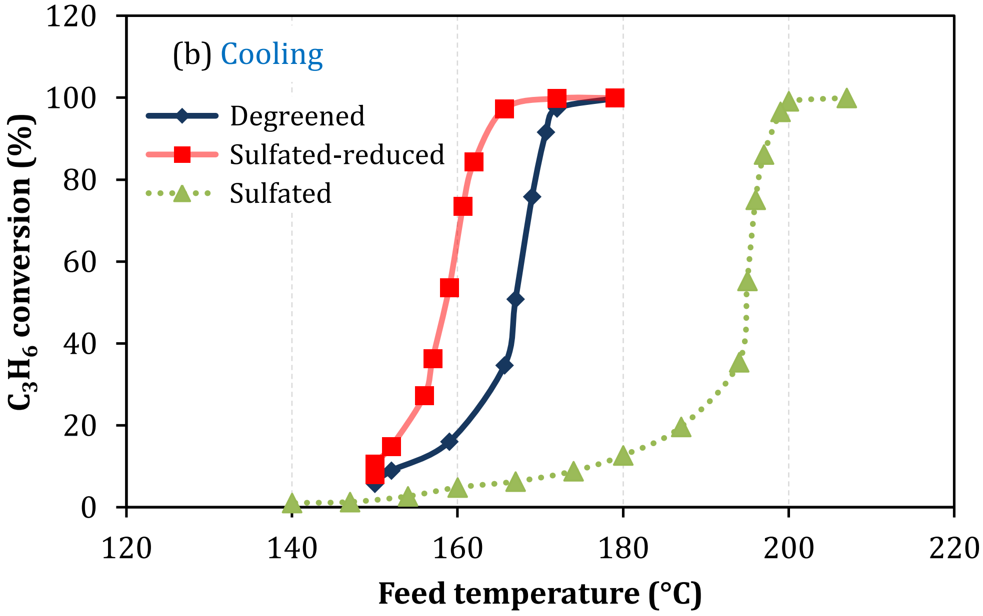

Figure 22: C_3H_6 conversion measured by temperature-programmed reaction (500ppm C_3H_6 + 8% O_2 + 5% H_2O) over Pt/Al_2O_3 degreened, sulfated (22h; 250°C; 30ppm SO_2 + 8% O_2 + 500ppm NO + 5% H_2O) and reduced after sulfation (1h; 500°C; 2% H_2). (a) Heating 5°C/min. (b) Cooling -5°C/min.

The sulfation also influenced the conversion hysteresis for both NO and C_3H_6 oxidation since it became larger indicating either a strong promotion during heating or a limiting effect during cooling. The activity measured after desulfation gave information to clarify this point. Indeed, after release of the most stable fraction of sulfur species (Figure 20), the NO oxidation activity during heating was not modified (Figure 23a), whereas the activity during cooling was improved by the absence of these surface species (Figure 23b).

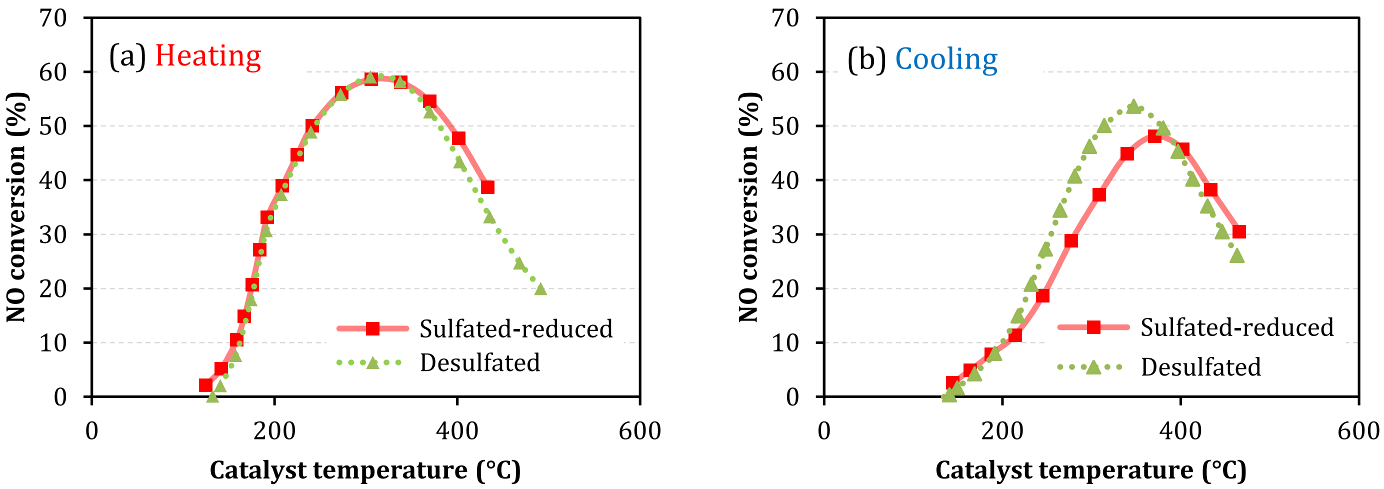

Figure 23: Effect of stable sulfur species created by SO_2 exposure on NO oxidation. The reduced catalyst contains the most stable species and the desulfated was sulfur-free. (a) Heating 5°C/min. (b) Cooling -5°C/min.

This result implies that the stable sulfur species, likely sulfates stored on alumina support, are able to interact during the cooling and decrease the activity. The migration of sulfates from the support to the active sites in operating condition is a possible way to explain this finding. After desulfation, similar conclusion can be drawn concerning propene oxidation, with an unchanged ignition activity and an improved extinction activity.

Chapter 7

Effect of the support and modification of the acido-basic properties

In diesel oxidation catalysts, like in most of heterogeneous catalysts, the active phase is dispersed on a support material, which provides high surface area, mechanical strength and thermal stability. The interaction between metal particles and the support is an important parameter to anchor and retain the metal and avoid deactivation due to particle growth. Metal oxides such as Al_2O_3, TiO_2, SiO_2 and ZrO_2 are widely used as catalytic supports. The support can be inert for the reaction or present reactive surface sites. Thus, Brønsted and Lewis acid sites are accessible on alumina (Al_2O_3) surface. These sites can for instance store molecules in reaction conditions and participate in the reaction.

Many Pt-based catalysts with various metal oxide supports have been screened for NO oxidation application. Schmitz et al. [16] evaluated the impact of various parameters such as Pt precursors, Pt loading and support on the NO oxidation activity. It was concluded that the support had the most important effect and SiO_2-supported Pt catalysts show higher rate than Al_2O_3 catalysts. The classification established by Benard et al. [15] regarding activity ranks the catalysts as follow: $Pt/SiO_2 > Pt/Al_2O_3 > Pt/CeO_2 > Pt/TiO_2 > Pt/ZrO_2 = Pt/YSZ = Pt/Al_2O_3\text{-}SiO_2$ which is in agreement with other studies [13, 16]. It is worth to note that the acid strength of Al_2O_3, SiO_2 and ZrO_2, evaluated by the color change of Hammett's indicators, follows the same trend since on a pKa scale: $SiO_2 < Al_2O_3 < ZrO_2$ [62]. There seems to be a correlation between support acidity and NO oxidation activity of supported-Pt catalysts. Yazawa et al. [62, 97-99] have described the effect of acidic metal oxide supports on the oxidation state of platinum. They demonstrated that acidic supports create an electron deficiency on platinum, which becomes therefore more resistant to oxidation.

7.1. Support modification by alkaline additives

To control the nature of the support, a mixed support material can be used and dopant can be added. Alkali and alkaline earths are additives that provide higher electron density to the catalysts and are able to improve the activity of Pt/Al_2O_3 towards lean NO reduction with C_3H_6 [31, 100].

The promotion by alkali and alkaline earth (Na, Ba, K, Rb, Li, Cs) has been described by Yentekakis et al. [31, 101] for the lean reduction of NO_x with various reductants over Pt and Pd-based catalysts. Na-promotion was particularly investigated and improved activity and N_2-selectivity at low temperature has been reported for NO reduction by propene [31]. Propene oxidation was also promoted by Na whereas NO oxidation was inhibited by the Na doping. High sodium loading, however, led to a complete suppression of NO reduction by propene.

The alkali promotion originates in the strengthening of the metal-NO bond along with the weakening of the N-O bond. In general, the increased electron density induced by the alkali promoter strengthens the metal-electron acceptor adsorbate bonds and reduces the strength of the metal-electron donor adsorbate bonds. The NO_x reduction by propene process suffers from the relative adsorption of NO and propene. Indeed, there is a competition between the two reactants to adsorb on the catalyst. An equal coverage of NO and C_3H_6 is desired to optimize the reaction rate but, in reality, propene adsorbs strongly on Pt/Al_2O_3 catalysts and covers the surface, which becomes inaccessible to NO. Na promotion enables to change the adsorption equilibrium by decreasing the propene adsorption ability and increasing NO adsorption. It was demonstrated that the Pt-O bond strength, known to play an important role in NO oxidation, was strengthened by alkali promotion. Strong Pt-O bond and platinum oxidation inhibits NO oxidation over Pt catalysts, which led us to examine the possibility of lowering the Pt-O bond strength.

7.2. Enhanced acidity by addition of chlorine

Chlorine belongs to the halogen group of elements and is therefore electronegative, i.e. it has a strong ability to drag electrons. The presence of chlorine in the catalyst composition can therefore decrease the electron density of the active metal and affect negatively the catalyst performance. However, the electronegativity of chlorine enhances the acidic nature of the catalyst [102], which is the wanted feature to carry out some catalytic reactions. Chlorinated alumina catalysts are employed in paraffins chemistry to perform acido-basic reactions such as isomerization, cyclisation, cracking [103-105]. During preparation, chlorine anions replace the hydroxyl groups of the alumina surface.

7.3. Sulfation to increase the catalyst acidity

Electro-attractor groups also influence the acido-basic nature of supported-metal catalysts. Thus catalysts can be modified by adsorption and storage of molecules such as SO_2. Extensive work has been performed on the effects of catalyst sulfation, which has been described as one way of preparing solid superacids, i.e. having an acidity higher than 100 % sulfuric acid [106]. The formation of adsorbed sulfur oxide complexes boosts the strength of acid sites. In order to identify the adsorbed species and the acido-basic centers, IR spectroscopy was widely used. Sulfate species absorb IR and the IR absorption of an appropriate probe molecule, adsorbed on the catalyst, enables to quantify and evaluate the strength of acido-basic sites. In particular, the complex structures, presented in Figure 24 generate strong acidity due to the S=O bonds that can readily accommodate an excess of electrons [106]. Yamaguchi et al. [106, 107] have identified the bidentate sulfate (A) species as the compound that is mainly responsible for the enhanced acidity, whereas Saur et al. [108] ruled out the formation sulfate (A) on Al_2O_3 and TiO_2. Instead Saur et al. inferred that the sulfate species responsible for acidity contained only one S=O bond and proposed the adsorption of species (B) (Figure 24) that can be converted in contact with water into Brønsted acid sites.

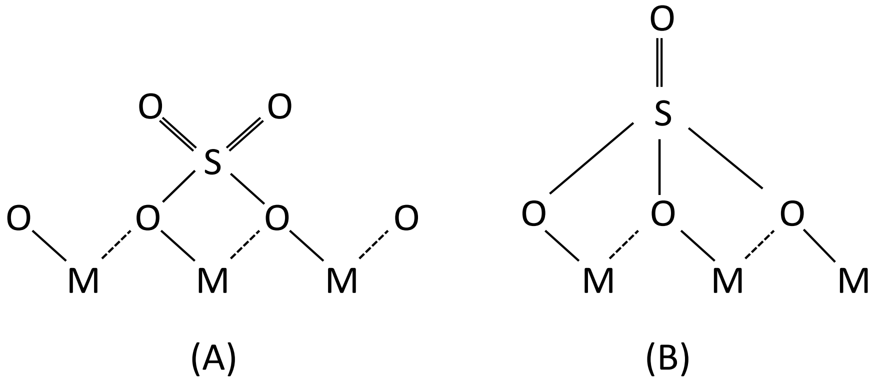

Figure 24: Configuration of sulfates adsorbed on metal oxide surface identified as acidity promoter.

The creation of Brønsted acid sites, absent on pure alumina, has been evidenced on sulfated alumina by the protonation of pyridine, a rather weak base [109, 110]. This new acidic centers conferred a better oxidation activity and a significant ability to cracking. Pure alumina however was more active for reduction than sulfated alumina. Przystajko et al. [109] postulated that sulfate groups destabilized adjacent hydroxyl groups and favored their protonation, generating the Brønsted sites. Sulfated zirconia showed very high acidity and good propane combustion activity has been achieved by Pt deposited onto this material [62]. The sulfate addition modified tremendously the nature of the catalyst since unmodified Pt/ZrO_2 catalyst was not active at all for the combustion of propane. The strength of weak Lewis acid sites of ZrO_2 and TiO_2 was increased by sulfation [110]. Fe_2O_3 is also greatly promoted by sulfation. The presence of sulfur in S^{6+} form generates indeed high acidity and high activity for cyclopropane isomerization [107].

7.4. Oxidation ability of an acidity-enhanced DOC

Two acidity-enhanced Pt/Al_2O_3 were prepared by chlorination and sulfation in acidic solution to evaluate the effect of support acidity towards NO and C_3H_6 oxidation. The first consequence of the acidic treatment was the increase of platinum dispersion compared to the unmodified Pt/Al_2O_3 catalyst. The temperature-programmed technique used to evaluate the effect of surface sulfur species was again employed.

NO oxidation

The degreened sulfated catalyst (M-S) and chlorinated catalyst (M-Cl) presented a lower oxidation activity than the standard degreened Pt/Al_2O_3 (M-Pt) during heating (Figure 25a). This is probably attributable to the poisoning of active sites by the excess of sulfate and chlorine rather than the enhanced acidity. However during cooling, unlike unmodified Pt catalyst, M-S and M-Cl showed a better NO oxidation activity than during heating (Figure 26), suggesting that the active sites were operational. Thus, during cooling, the sulfated sample turned out to be the most active, while M-Cl and M-Pt displayed very similar activity profiles (Figure 25b).

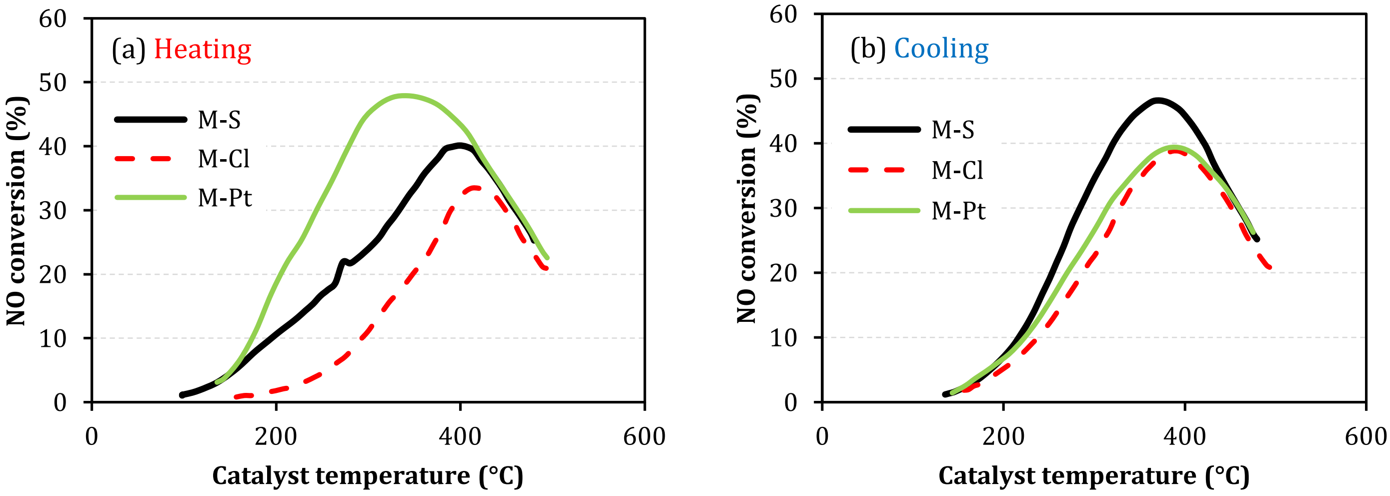

Figure 25: NO conversion comparison (500ppm NO + 8% O_2 + 5% H_2O) between chlorinated Pt/Al_2O_3 (M-Cl), sulfated Pt/Al_2O_3 (M-S) and unmodified Pt/Al_2O_3 (M-Pt) during (a) heating (5°C/min) and (b) cooling (-5°C/min).

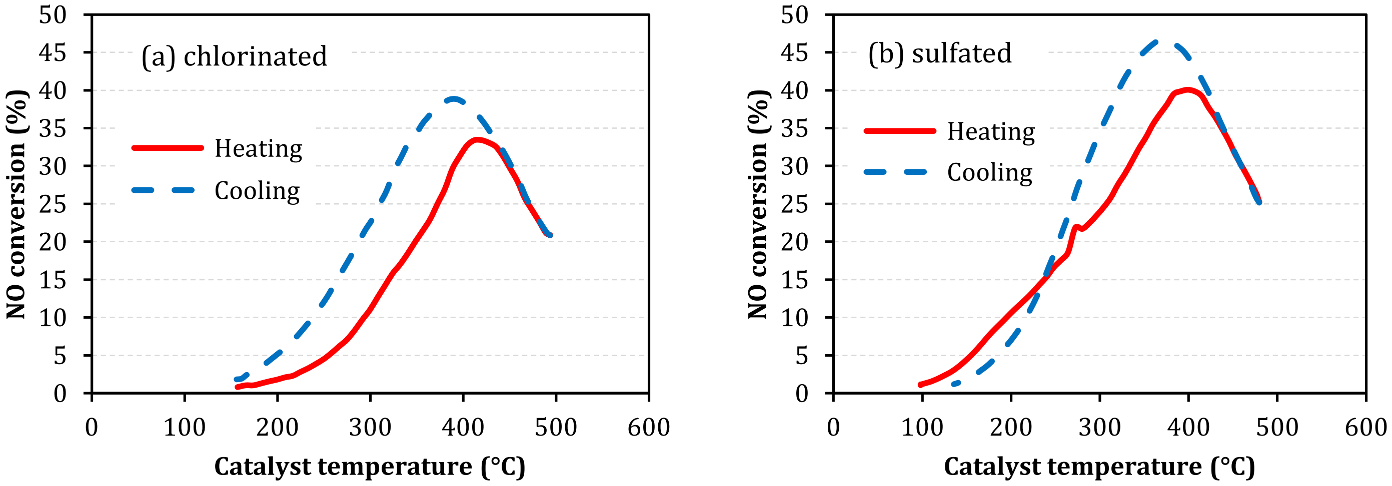

Figure 26: NO conversion profiles (500ppm NO + 8% O_2 + 5% H_2O) during heating (5°C/min) and cooling (-5°C/min) of (a) chlorinated Pt/Al_2O_3 (M-Cl) and (b) sulfated Pt/Al_2O_3 (M-S).

The conclusion that can be drawn from the results reported above is that enhanced acidity limits the deactivation of the catalyst due to platinum oxide formation usually observed during cooling. The electroattraction of sulfates and chlorine groups decrease the electron density of platinum particles and thus decreases platinum ability to bind strongly oxygen atoms. Sulfation proved to be more efficient than chlorination for this purpose.

C_3H_6 oxidation

After NO oxidation, propylene oxidation was performed over each of the three catalysts (M-Pt, M-S, M-Cl). The three activity profiles are comparable during heating (Figure 27 a), which indicates that the species that caused the initial low NO oxidation performance were removed. It also means that propene combustion is affected only to a small extent by the enhanced support acidity. However, during cooling, there is a trend showing the slight negative effect of enhanced acidity on propylene combustion (Figure 27 b). This result is in line with the improved propene oxidation obtained by alkaline doping by Yentekakis et al. [31] since, in our case, the electron density of Pt is expected to be lowered.

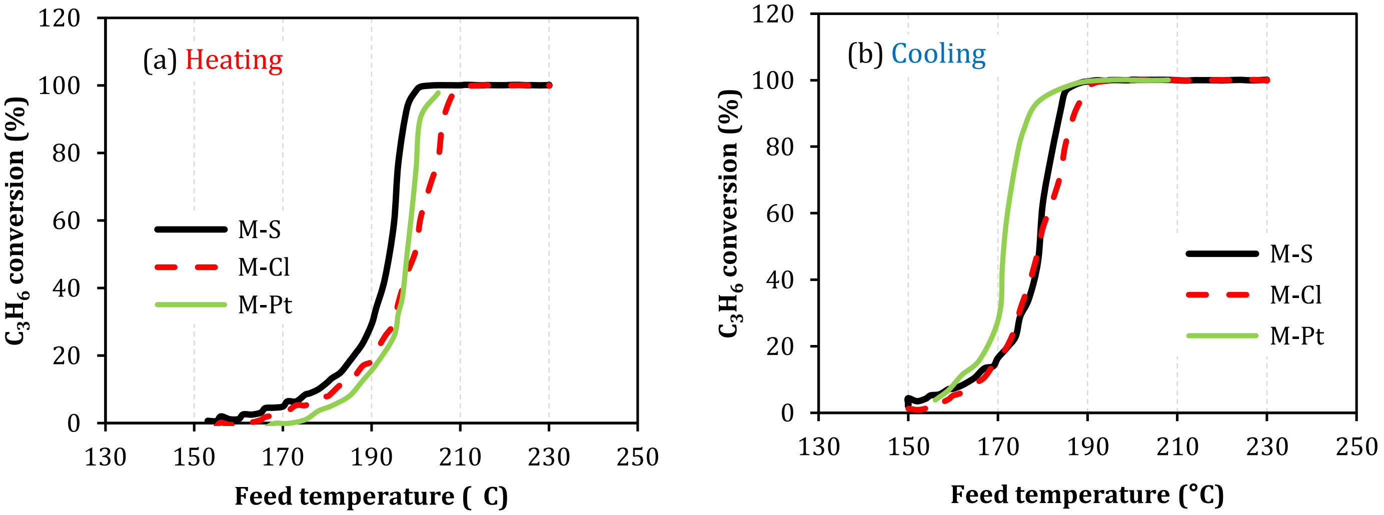

Figure 27: C_3H_6 conversion comparison (500ppm C_3H_6 + 8% O_2 + 5% H_2O) between chlorinated Pt/Al_2O_3 (M-Cl), sulfated Pt/Al_2O_3 (M-S) and unmodified Pt/Al_2O_3 (M-Pt) during (a) heating (1°C/min) and (b) cooling (-1°C/min).

7.5. SO_2 aging of chlorinated and sulfated catalysts

The acidity-enhanced catalysts were aged for 22 h at 250°C in the following gas mixture: 500 ppm NO + 8 % O_2 + 30 ppm SO_2 + 5 % H_2O diluted in argon (3 L/min). They were then reduced for one hour at 500°C in 2% H_2. The aging and reduction procedure increased the oxidation ability of M-Cl and M-S as it does for the unmodified Pt/Al_2O_3 catalyst. However, it can be seen that both catalysts were less active during cooling for NO oxidation (Figure 28) and therefore followed the usual trend observed for Pt/Al_2O_3 catalyst. That suggests the loss of their acidic properties during aging that conferred a protection against Pt oxides formation.

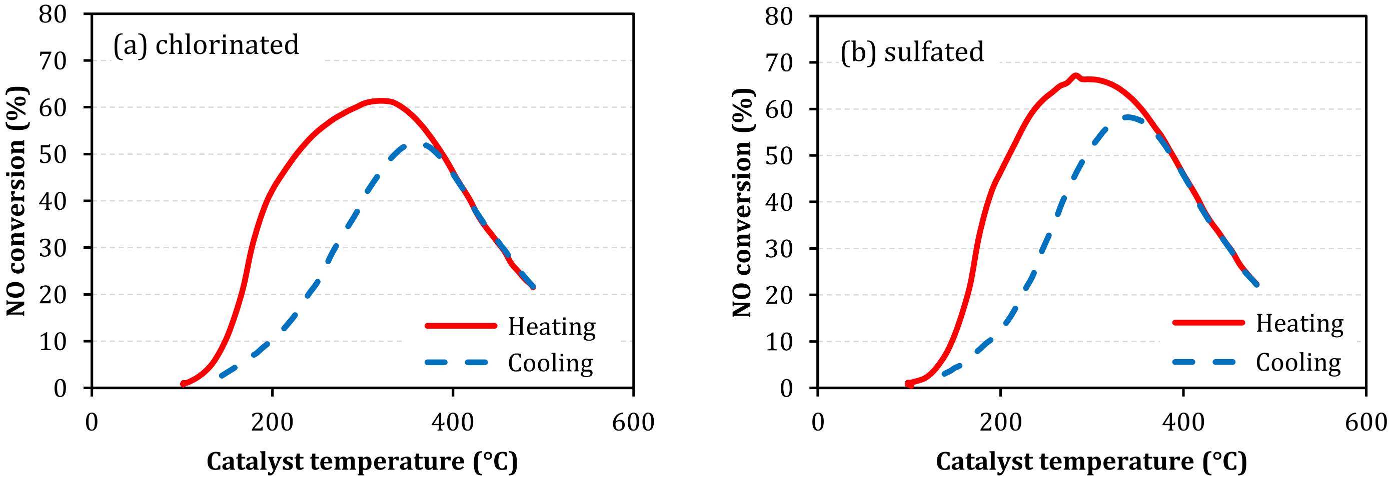

Figure 28: NO conversion profiles (500ppm NO + 8% O_2 + 5% H_2O) during heating (5°C/min) and cooling (-5°C/min) of (a) chlorinated Pt/Al_2O_3 (M-Cl) and (b) sulfated Pt/Al_2O_3 (M-S) after aging with 500ppm NO + 8% O_2 + 30ppm SO_2 + 5% H_2O and reduction.

7.6. SO_2 storage of chlorinated and presulfated Pt/Al_2O_3

Similar sulfation treatment as described in Paper I and III was carried out to assess the SO_2 storage capacity of chlorinated and presulfated Pt/Al_2O_3. Subsequently, one reduction step at 500°C was performed in order to remove and quantify the less stable species and one TPR up to 800°C was conducted to remove the most stable species. The results of the sulfur release are presented in Figure 29 and 30. In general, the sulfur storage is lower on acidity-enhanced catalyst than on unmodified Pt/Al_2O_3 (Figure 29). Silica, which is more acidic than alumina, is known to be insensitive to SO_2, which is line with our results. The distribution between less and more stable sulfur species is interesting since it differs greatly between samples. While on Pt/Al_2O_3 the two types of species were released in equivalent amount, important difference exists in their respective proportion on M-S and M-Cl, as shown in Figure 29. M-S released a high amount of low-stability species that corresponds to the maximum observed among the three catalysts. However a small amount of sulfur, compared to M-Pt and M-Cl (Figure 30), was released during TPR, indicating a low amount of stable species. A fraction of released sulfur likely originates from the sulfates deposited in the catalyst preparation. That might explain the high amount of less stable species. On M-S, the presence of a third type, more stable, of sulfur species, which is not released during TPR, cannot be ruled out. The chlorinated catalyst, M-Cl, was the only catalyst that released more sulfur during the TPR than during the reduction at 500°C. The amount of less stable species was particularly low, indicating that chlorine prevented the formation of this kind of species. The release during TPR was interestingly very similar to the release recorded for M-Pt (Figure 30). This feature suggests that chlorine influenced neither the formation nor the stability of such sulfur species.

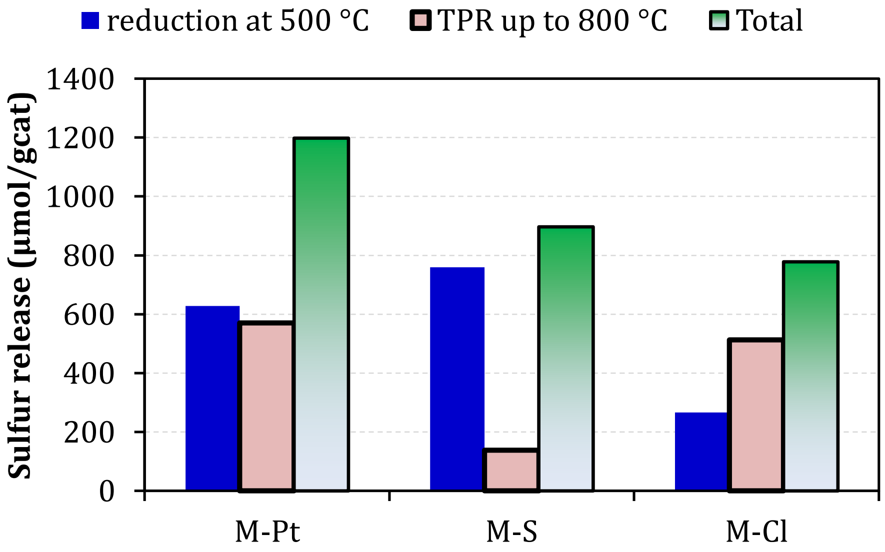

Figure 29: Stepwise sulfur release showing the distribution and stability of species formed during sulfation of chlorinated (M-Cl), pre-sulfated (M-S) and unmodified Pt/Al_2O_3 (M-Pt).

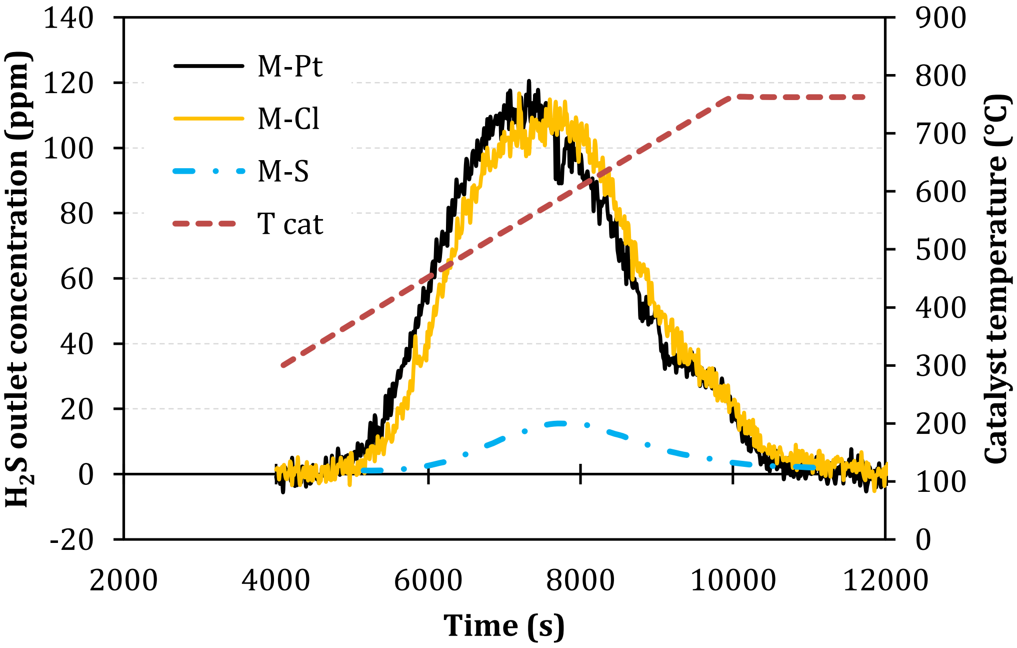

Figure 30: H_2S release during Temperature-Programmed Reduction up to 800°C (TPR) in 2% H_2 of M-Cl, M-S and M-Pt.

Chapter 8

Intra-catalyst insight of SCR with NH_3 on Cu-BEA

8.1. Experimental measurements

NH_3-SCR was carried out on a Cu-Beta zeolite prepared at Chalmers containing 4.3 wt.% copper. The catalyst was characterized following a 4-step protocol developed by Cummins to study several reactions occurring in operating conditions [111]:

1. NO oxidation	**$2\ NO + O_2 \leftrightarrow 2\ NO_2$**
2. NO reduction by NH_3	**$4\ NO + 4\ NH_3 + O_2 \leftrightarrow 4\ N_2 + 6\ H_2O$**
3. NH_3 oxidation	**$4\ NH_3 + 3\ O_2 \leftrightarrow 2\ N_2 + 6\ H_2O$**

NH_3 storage in presence and absence of NO was also studied and the storage capacities of the catalyst were determined. The SpaciMS analysis gave the spatial distribution for all of these features. The 4-step protocol consisted in changing the gas composition of the feed by turning NH_3 and/or NO supply on and off in order to investigate NH_3 storage and the reactions mentioned above. The description of the protocol is given in Table 1.

Table 1: Feed composition during each step of the 4-step protocol (total flow 510 sccm).

	NO_X	NH_3	O_2	H_2O	Kr
Step1 (NO oxidation)	205ppm	0	10%	5%	100ppm
Step2 (SCR)	205ppm	183ppm	10%	5%	100ppm
Step3 (NH_3 oxidation)	0	183ppm	10%	5%	100ppm
Step4 (NO oxidation)	205ppm	0	10%	5%	100ppm

In order to simulate real conditions, the gas feed contained 10 % O_2, 5 % H_2O throughout the whole protocol. Krypton was added for MS signal analysis and correction. The water vapor was generated by evaporation of liquid water heated at a fixed temperature in a hot bath. The vapor was then carried by a flow of Ar. In the first step, 205 ppm NO was added to the base stream to clean the surface of adsorbed NH_3 as well as studying the NO oxidation. In step 2, NO was kept in the flow and 183 ppm NH_3 was added in order to perform the SCR reaction described in chapter 4 as well as studying the dynamic of NH_3 storage in operating conditions. When the SCR reaction reached steady state, NO was turned off, marking the start of step 3. In this step, the storage of NH_3 in the absence of NO was studied and the reaction of NH_3 oxidation was observed. Finally in step 4, NH_3 was switched off and NO was simultaneously started in order to observe the reaction occurring between the flowing NO and NH_3 stored on the surface. The total storage capacity of the catalyst could be determined by the consumption of NO and the release of NH_3 in this last step. After the fourth step, NO and NH_3 were turned off in order to get a baseline of concentrations for subsequent calculations. The capillary was then translated to the next measurement position and the 4-step protocol could be run at this new location. Before moving on to the next position, the protocol was repeated twice and the results from the second cycle were analyzed.

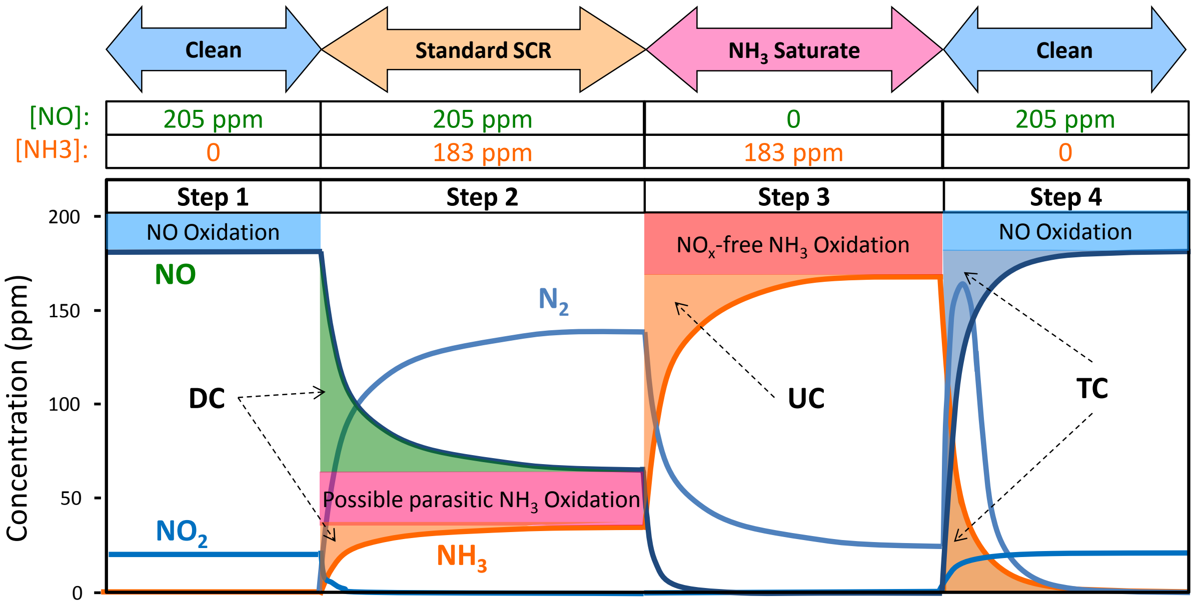

Figure 31: Schematic experimental concentration profiles during the 4-step protocol and representation of storage capacity integration. DC is the dynamic storage capacity, observed during SCR, UC refers to the unused capacity, measured during NH_3 oxidation, and TC stands for total capacity.

8.1.1. NO and NH_3 oxidation

Cu-zeolite catalysts are active for oxidation of NO and NH_3, which was verified in step 1 and 3 of our protocol (Figure 31), respectively. Ammonia oxidation reaction can interfere during SCR by consuming ammonia and therefore needs to be controlled in order to adjust the injection of urea (precursor of NH_3) necessary to reduce NO_x, in practical application. NO oxidation is important, since it produces NO_2 and therefore changes the rate and mechanism of SCR reaction from ¨Standard SCR¨ to ¨Fast SCR¨ or ¨NO_2-SCR¨. It has been proposed that NO oxidation was in fact the rate determining step (RDS) of the SCR reaction [50]. However, other studies have suggested that this is not the case. For example H_2O has a detrimental effect on NO oxidation, but only minor impact on the SCR rate [112], which suggests that NO oxidation is not the RDS. With the use of spatially resolved measurements, the extent of reaction along the monolithic catalyst was evaluated (Figure 32).

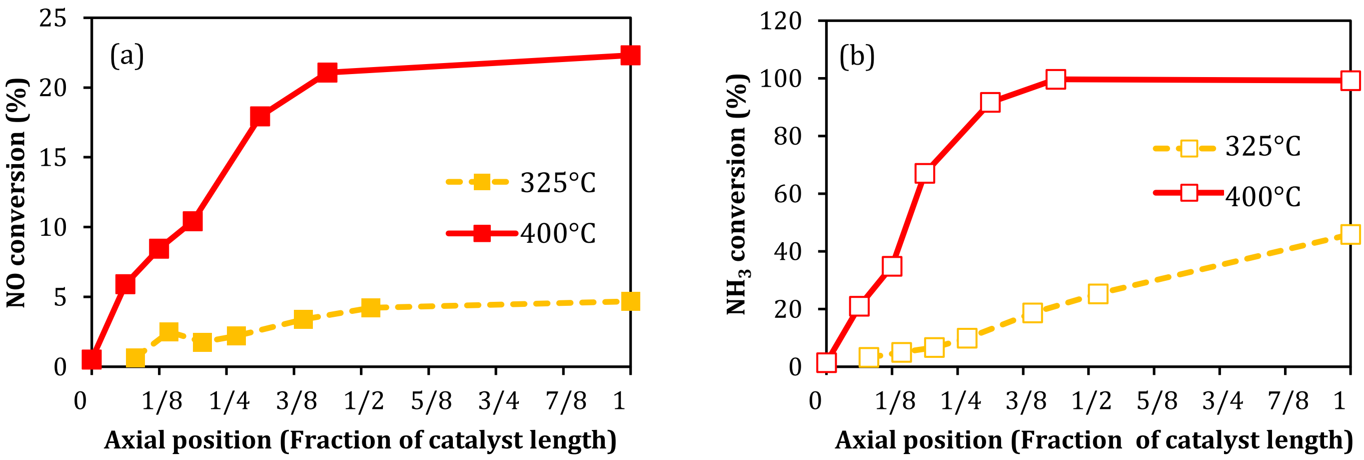

Figure 32: Performance of the Cu-BEA SCR catalyst at 325°C and 400°C for (a) NO oxidation and (b) NH_3 oxidation, presented as the conversion throughout the catalyst (0=inlet, 1=outlet).

The catalyst is more active at higher temperature for both oxidation reactions and did not show any activity at 200°C. NO oxidation increased in the front half of the catalyst (Figure 32 a) and then stabilized due to the inhibition effect and the dissociation of NO_2. The NO conversion reached at 400°C was 23 %. Higher activity was noted for NH_3 oxidation as seen in Figure 32 b. At 325°C, NH_3 conversion increased almost linearly from the inlet to the outlet where it exhibited a maximum at 45 %. At 400°C a sharp conversion increase was observed in the front part leading to the total NH_3 conversion by the half catalyst position.

8.1.2. Selective catalytic reduction of NO by NH_3

Contrary to NH_3 and NO oxidation, the SCR occurred at all three temperatures. SCR was studied during step 2 and was evidenced at the start of step 4. The amount of catalyst used to reach 100 % conversion, the NH_3:NO stoichiometry and the N_2O production were especially considered.

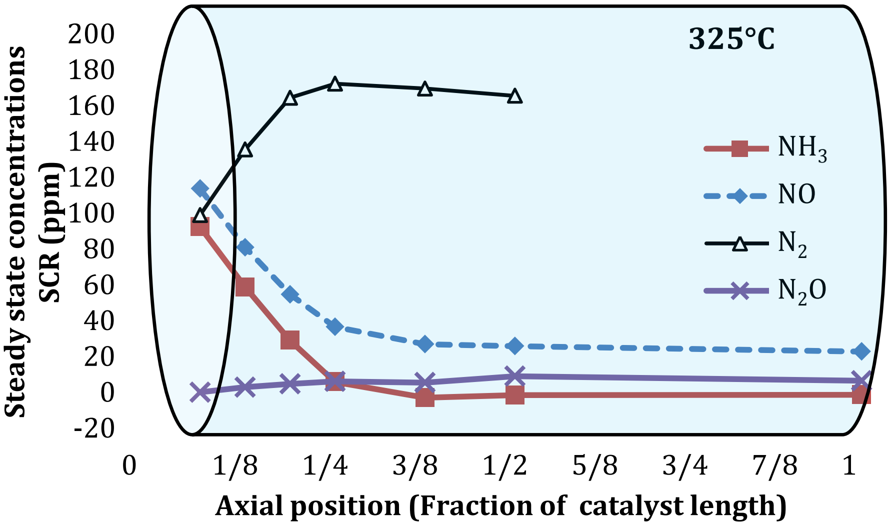

Figure 33: Steady state evolution of NO, N_2, NH_3 and N_2O concentrations during SCR at 325°C (205ppm NO + 183ppm NH_3 + 10% O_2 + 5% H_2O)

Since the feed contained less NH_3 than NO, the conversion of NO was normalized to the inlet NH_3 concentration as:

$$\chi_{NO} = \frac{[NO]^{in} - [NO]^{out}}{[NO]^{in}} * \frac{[NO]^{in}}{[NH_3]^{in}} \qquad \text{(Eq. 8.1)}$$

This normalized NO conversion can be directly compared to NH_3 conversion to assess the stoichiometry of the reaction. In Figure 34, it can be seen that the NH_3 conversion and the normalized NO conversion profiles are very close, which means that as much ammonia as nitric oxide disappears and, consequently the stoichiometry of the SCR reaction over our Cu-BEA catalyst is NH_3:NO=1. Even at 400°C (Figure 34 c), where NH_3 oxidation is fast, over-consumption of ammonia was not observed. This is likely due to that the SCR rate was significantly higher than NH_3 oxidation rate at this temperature. In these conditions, 100 % conversion was reached at the outlet at all three temperatures and effluent-based analysis would not be able to display the rate differences. However, the SpaciMS technique revealed important information about the kinetics of SCR reaction. Indeed, Figure 34 shows that the SCR zone, defined as the length of catalyst necessary to convert 100 % of NO, becomes shorter and condensed to the front as the operating temperature increases from 200°C to 400°C. These kinetics data, acquired in realistic conditions, are valuable for the development of a kinetic model.

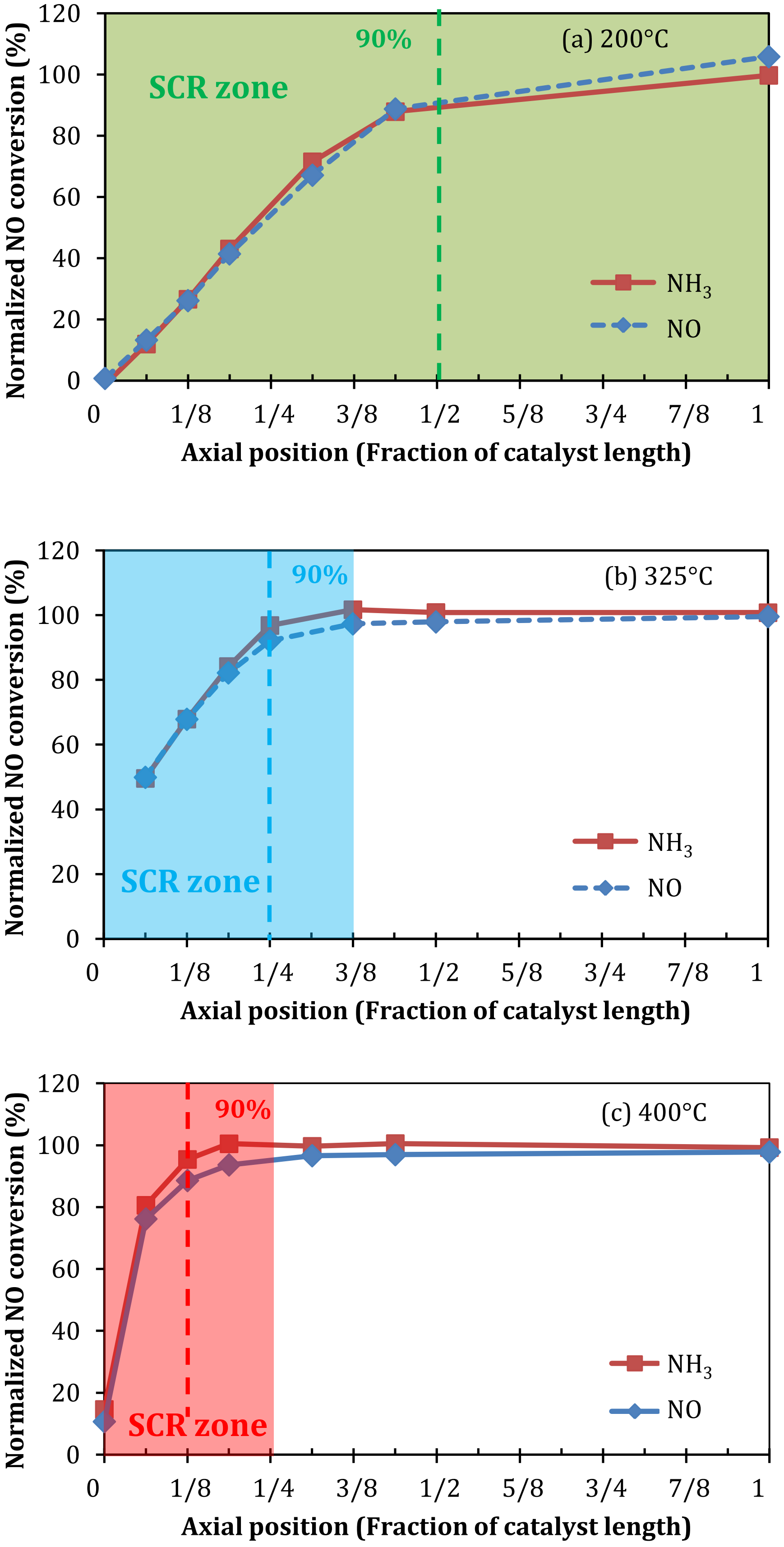

Figure 34: NO and NH$_3$ conversion during SCR (step 2) with highlight on the SCR zone at (a) 200°C, (b) 325°C and (c) 400°C.

The major products of SCR are N_2, which is wanted and N_2O, which must be as low as possible due to its high global warming potential (~300 times higher than CO_2). The production of N_2O has been found non-monotonic with respect to the temperature. Indeed, the outlet concentration of N_2O was higher at 200°C and 400°C than at 325°C (Figure 35). This result suggests the possibility of multiple mechanisms to form N_2O in order to describe N_2O at both high and low temperature. At low temperature, decomposition of ammonium nitrate has been proposed to be the main source of N_2O [46, 51, 113]. At high temperature, on Fe-zeolite, N_2O formation has been correlated to NO_2 [46, 50, 114]. On Cu-zeolite, copper dimer sites have been found responsible for N_2O production at high temperature [113].

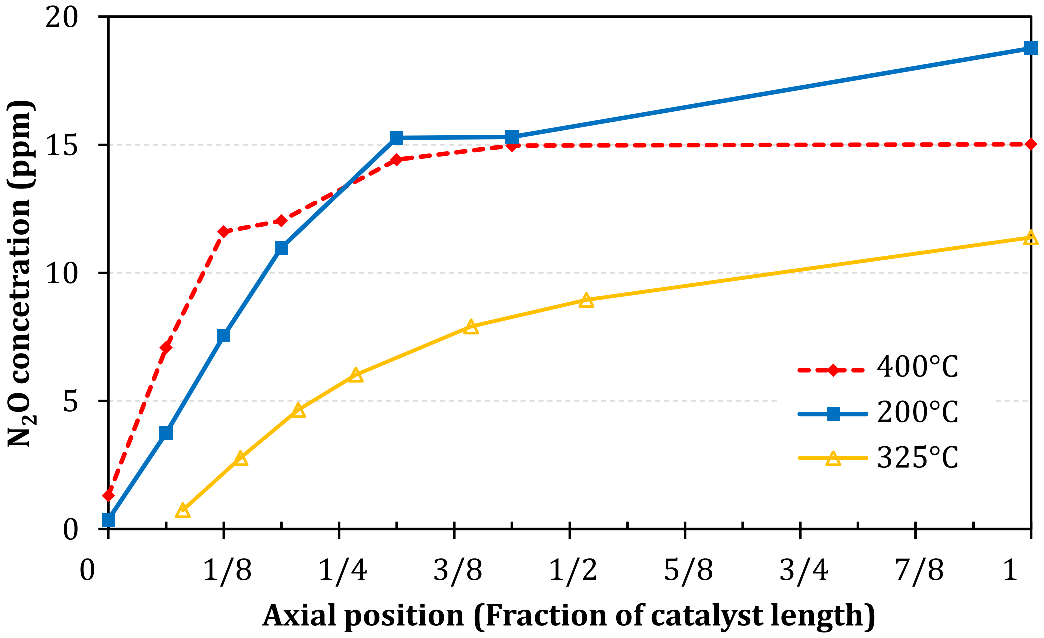

Figure 35: Steady state N_2O concentration profiles during SCR step 2 at 200°C, 325°C and 400°C.

8.1.3. NH_3 storage capacity

The NH_3 storage capacity of the catalyst was studied in presence and absence of NO. In step 2, NO, NH_3 and oxygen were flowing and SCR occurred. In parallel, NH_3 was stored on the catalyst, which defined the dynamic storage capacity (DC) of the catalyst at a particular position. The unused capacity (UC) was obtained by integrating the NH_3 storage during step 3, without NO. The total storage capacity (TC) could be determined in two ways: by addition of the dynamic and the unused capacity DC+UC or by direct measurement in step 4, when the stored NH_3 was either released or converted into N_2 and N_2O.

The integrated area representing the storage capacities are shown in Figure 31. The total storage capacity increases with decreasing the temperature. At 400°C, no storage could have been measured. The storage distribution between dynamic and unused capacity depends, however, on the axial position. TC was inferred from step 4 where stored NH_3 was quickly released or quickly reacted under the action of NO to form N_2. The consumption of NO and the NH_3 release in step 4 were used to determine the total storage capacity. DC, as indicated in Figure 31, was calculated in step 2 by integration of NO and NH_3 signals, relative to steady state level. The storage (DC and TC) at 200°C and

325°C is represented in Figure 36. It can be noticed that in the front of the catalyst, DC and TC are very similar, which reveals that all storage sites were filled during SCR. It also means that the SCR reaction does not affect the ammonia storage and both processes occur simultaneously, which is an important information regarding the dynamic behavior of the SCR catalyst. The two curves separate at a location that corresponds to the 90 % NO conversion zone, when DC remains almost constant while TC keeps increasing. Indeed, downstream of the SCR zone, no ammonia remains in the gas phase and no ammonia storage can be detected. This is in agreement with our experimental results displaying constant DC after the SCR zone.

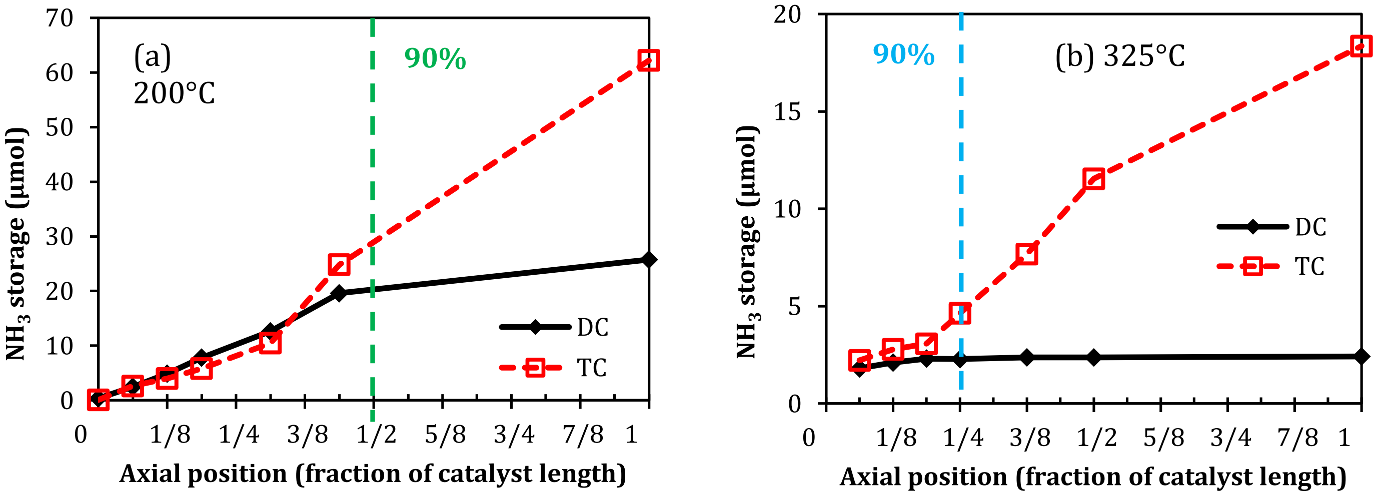

Figure 36: Ammonia dynamic storage capacity measured during SCR step (DC) and total storage capacity measured in step 4 (TC). (a) at 200°C and (b) at 325°C. The respective position of 90 % NO conversion is displayed on the figures.

8.2. Kinetic modeling simulations

Kinetic modeling applies kinetic theory and chemical reaction engineering to evaluate the rate of a reaction in desired operating conditions. Kinetic modeling can be used to find empirically reaction kinetic parameters; it can provide information about reaction mechanism and can help to determine the rate determining step of a complex reaction, which is especially applicable to catalytic reactions. Many kinetic models assuming different mechanisms have been developed to describe NH_3-SCR [115-121]. Experimental data used to fit the kinetic parameters are usually based on effluent gas composition over a wide range of initial conditions and temperature. We developed a kinetic model based on steady state intra-monolith concentration profiles. The kinetic parameters were tuned in order to simulate axial concentration evolutions that match the experimental measurements.

The simulations were carried out with the commercial software AVL BOOST Aftertreatment in connection with a user-defined Fortran script, in which reaction rate equations and parameters were defined. The system was reduced to one channel, assuming all channels identical, and discretized in a series of 15 elements, in which the mass balance (Eq. 8.1) of each species was solved

$$\varepsilon_g \cdot \frac{\partial \rho_g \cdot w_{k,g}}{\partial t} = \varepsilon_g \cdot \frac{\partial \rho_g \cdot w_{k,g} \cdot v_g}{\partial z} + \varepsilon_g \cdot \frac{\partial}{\partial z}\left(\rho_g \cdot D_{eff} \cdot \frac{\partial w_{k,g}}{\partial z}\right) + MG_{k,g} \cdot \sum_i^I \nu_{i,k} \cdot \dot{r}_i(c_k^L, T_s) \qquad \text{(Eq. 8.2)}$$

where $w_{k,g}$ is the mass fraction of species k, D_{eff} is an effective diffusion coefficient, $r_i(c_k^L, T_s)$ represents the molar reaction rate of the surface reaction i, $\nu_{i,k}$ is the stoichiometric coefficient of the species k in the reaction i and ε_g is the volume fraction of the gas phase in the total volume. Considering the low working temperature range, homogeneous gas phase reactions were negligible and not taken into account in the model. The transport from the gas phase to the washcoat was described by the film transport model. The Arrhenius equation (Eq. 8.3) was applied to express the temperature-dependence of the rate constant of the considered reactions.

$$k = A\, exp\left(-\frac{E_A}{RT}\right) \qquad \text{(Eq. 8.3)}$$

The kinetic parameters A (pre-exponential factor) and E_A (activation energy) were tuned to obtain the best fit to experimental intra-catalyst concentration profiles based on steady state values. Before fitting parameters related to NH_3-SCR (step 2 in the protocol), NO oxidation, NH_3 adsorption/desorption and NH_3 oxidation were independently studied. NO and NO_2 concentrations measured in step 1 were used to determine adequate parameters for NO oxidation. NO oxidation was simulated in the model as a global gas phase reaction (r3 in Table 2), which do not imply an actual gas phase mechanism but is a simplification in the model. In the same way, NH_3 and N_2 steady state profiles were used to fit ammonia oxidation parameters. This reaction was represented in the model by a reaction between O_2 in the gas phase and adsorbed NH_3 (r2 in Table 2), which again is only a simplification in the global kinetic model. The adsorption and desorption process (r1 in Table 2) was studied in an independent experiment consisting in adsorption of NH_3 at 40°C followed by a temperature ramping up to 600°C to release the stored ammonia. The site density was tuned to fit the ammonia release during the ramping phase. The coverage-dependence of the activation energy of ammonia desorption was taken into account. It was thus expressed using a Temkin isotherm, which considers the adsorbate - adsorbate interactions: (Eq. 8.4):

$$E_{NH_3,des} = E^0_{NH_3,des}\,(1-\alpha\,\theta_{NH_3}) \qquad \text{(Eq. 8.4)}$$

where α is a constant, θ_{NH_3} the coverage and $E^0_{NH_3,des}$ the activation energy for 0 coverage. This expression was employed in many kinetic models [118-120] and agrees with Wilken et al. [122] micro-calorimetry results. The coverage dependent heat of adsorption was determined in micro-calorimetry experiments ($112.75*(1-0.39*\theta_{NH_3\text{-}S1})$). The SCR parameters as well as the N_2O formation parameters were simultaneously tuned to fit the observed steady state concentrations at the end of step 2. Two mechanisms for N_2O production were included in the model to describe the higher yields obtained at 200°C and 400°C compared to 325°C, which cannot be described by one single Arrhenius reaction. The “low temperature” route proposed is a two-step process starting with the formation of an intermediate “NH_3-NO” adsorbed species that decomposes in a subsequent step into N_2O, N_2 and H_2O according to reaction 6 and 7 in Table 2.

Table 2: Reaction steps and rate expressions included in the kinetic model.

Nb	Reactions	Rate expression
1	$NH_3 + S1 \leftrightarrow NH_3\text{-}S1$	$r_1 = k_{1f} * \theta_v * [NH_3] - k_{1b} * \theta_{S1\text{-}NH3}$
2	$4NH_3\text{-}S1 + 3O_2 \rightarrow 2N_2 + 6H_2O + 4\ S1$	$r_2 = k_2 * \theta_{S1\text{-}NH3} * [O_2]$ ^ $\beta 1$
3	$NO + 0.5\ O_2 \leftrightarrow NO_2$	$r_3 = k_{3f} * [NO] * [O_2]$ ^ $0.5 - k_{3b} * [NO_2]$
4	$4NH_3\text{-}S1 + 4NO + O_2 \rightarrow 4N_2 + 6H_2O + 4S1$	$r_4 = k_4 * \theta_{S1\text{-}NH3} * [NO] * [O_2]$ ^ $\beta 2$
5	$2NH_3\text{-}S1 + 2NO + O_2 \rightarrow N_2O + N_2 + 3H_2O + 2S1$	$r_5 = k_5 * \theta_{S1\text{-}NH3} * [NO] * [O_2]$
6	$NH_3\text{-}S1 + NO \leftrightarrow (S1)\text{-}NH_3\_NO$	$r_6 = k_{6f} * \theta_{S1\text{-}NH3} * [NO] * \theta - k_{6b} * \theta_{S1\text{-}NH3\_NO}$
7	$2\ S1\text{-}NH_3\_NO + O_2 \rightarrow N_2O + N_2 + 3\ H_2O + 2S1$	$r_7 = k_7 * \theta_{S1\text{-}NH3\_NO} * [O_2] * \theta_v$

The reaction order of oxygen β1 and β2 were determined in experiments with varying oxygen concentrations to 0.6 and 0.5, respectively.

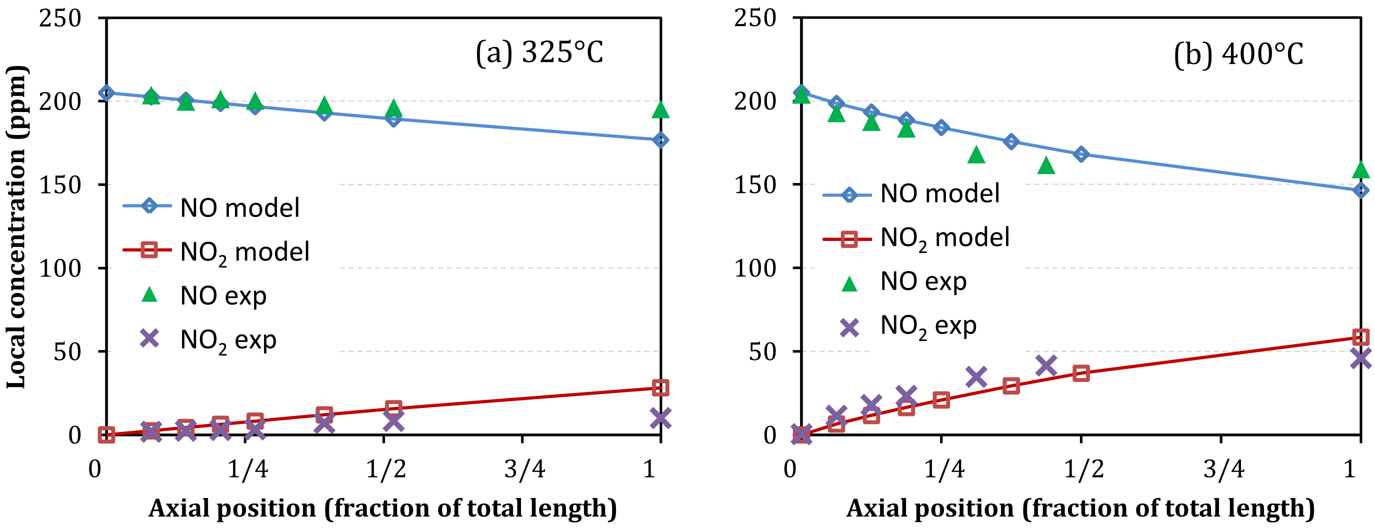

Figure 37: Experimental and simulated steady state NO and NO_2 concentration profiles during NO oxidation (step 1). (a) at 325°C and (b) at 400°C.

To reduce the number of parameters to be fitted, some kinetic parameters were set to literature values. That was the case for the activation energy of NO oxidation reaction, which was set to 48 kJ/mol according to Olsson et al. [117]. Only the pre-exponential factor was therefore tuned for that reaction, which led to an adequate curve fit both at 325°C and 400°C, as seen in Figure 37. However, the activation energy for ammonia oxidation reported by Sjövall et al. [118] (162.5 kJ/mol) was too high to fit with a good agreement our spatial experimental data. Table 3 summarizes the reaction steps and their respective parameters used in the model. NH_3 adsorption as well as NH_3-NO complex formation are non-activated reversible steps. The model predicted the experimentally observed SCR stoichiometry, in other words, the absence of ammonia over-consumption. NH_3 over-consumption was observed over Fe-zeolite catalysts [50, 116, 123] and is a crucial parameter in dosing NH_3 injection.

Table 3: Summary of kinetic parameters used in the kinetic model.

Reaction	Pre-exponential factor [a]	Activation energy (kJ/mol)
NH_3 adsorption	9279	0
NH_3 desorption	6.76e8	112.75
NH_3 oxidation	8.00e8	130.0
NO oxidation	1.10e5	48.0
SCR	2.50e8	60.0
N_2O formation “high temperature”	1.90e16	160.0
N_2O formation “low temperature” complex formation	65	0
N_2O formation “low temperature” complex dissociation	8.48e10	65.0
N_2O formation “low temperature” complex decomposition	7.33e18	95.0

[a] The unit of the reaction rate is kmol/(m^3·s) and the gas phase concentration are dimensionless.

The model validation was based on the transient response to gas composition changes when the whole 4-step experiment was simulated. The model describes the experimental features adequately. One example of full experiment simulation, at 200°C and 1/4 of catalyst is shown below (Figure 38).

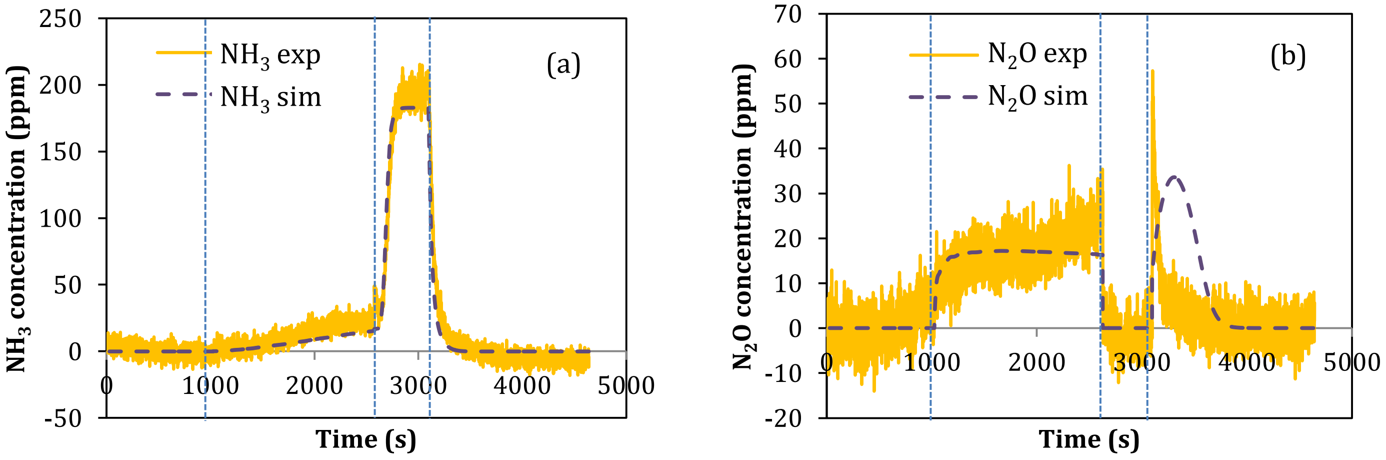

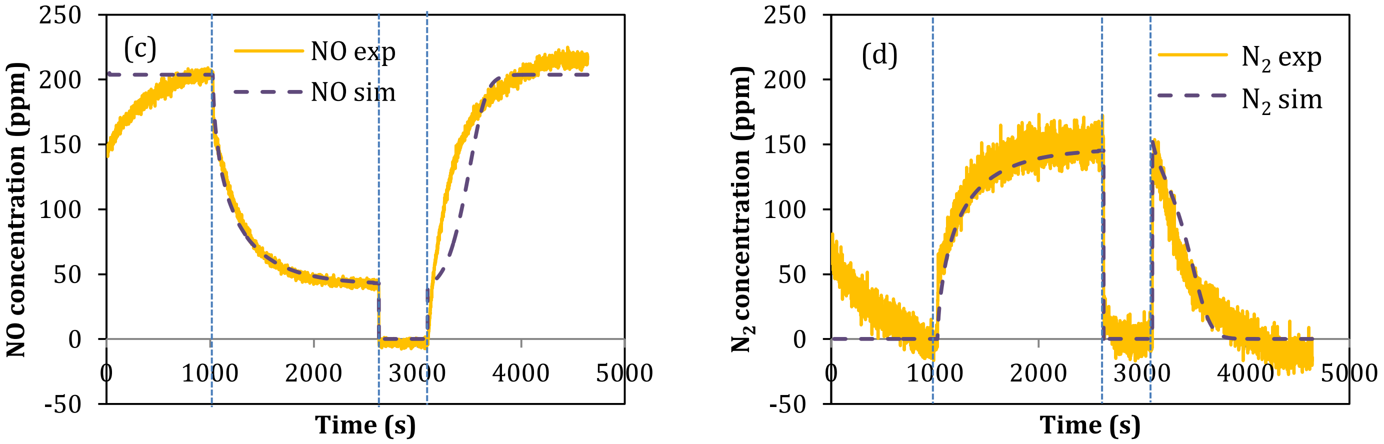

Figure 38: Comparison of simulated and experimental concentration profiles for (a) NH_3 , (b) N_2O , (c) NO and (d) N_2 at 200°C and 1/4 monolith length from the inlet.

At this position, the steady state concentration of all components and in all the four steps is in line with the experimental data. The transient evolution in step 2 is captured well by the model for all components. The ammonia storage indicated in step 3 by the time to reach ammonia signal steady state is accurately modeled. However, the model predicts too high NO consumption and N_2 and N_2O production in step 4. These conclusions differ depending on the considered temperature and location but the simulated results agree well with the experimental data, in general.

Chapter 9

Concluding remarks

In this thesis, two major aspects of diesel emission control were addressed. A typical diesel oxidation catalyst and a lean NO_x reduction catalyst were studied during flow reactor experiments. The activity response of the model DOC to aging treatment and sulfur poisoning was specifically investigated. The performance of the SCR catalyst was evaluated with intra-monolith spatially resolved measurement and was used to develop a kinetic model.

Aging an alumina-supported Pt catalyst at high temperature in various atmospheres revealed the faster sintering of Pt particles in presence of SO_2. In contrast, H_2 seemed to prevent sintering up to 700°C. In oxidative and inert flow, the dispersion decreases with aging temperature with similar linear trend. Long aging at lower temperature (250°C) in presence of water, oxygen and SO_2, followed by reduction in H_2, led to significant dispersion loss and simultaneous activity improvement for both NO and C_3H_6 oxidation. The role of surface sulfur stored during the aging step was investigated in order to attempt to explain the resulting catalytic activity. Two types of sulfur species characterized by different stability and reducibility were identified on the catalyst after aging. The less stable species could be removed by reduction treatment at 500°C but had a major detrimental effect on oxidation performance. Nevertheless, our results indicate that these species are mobile and can be replaced on the active sites by NO provided that the operating temperature is high enough. The second type of sulfur species, more stable, was decomposed at higher temperature to form H_2S and could likely be assigned to sulfates stored on the alumina support. The effect of the stable sulfur adsorbates is minor and affects only the activity during extinction suggesting their migration from the support to the active sites at elevated temperature. Since the presence of adsorbed sulfur species causes an activity loss, our results suggest that the beneficial effect of SO_2 aging is due to sulfur-assisted platinum sintering. It would be interesting to reproduce similar SO_2 aging study on Pd and bimetallic Pd-Pt-based catalysts since commercial DOCs contain also palladium. Bimetallic Pd-Pt catalysts are known to be more resistant to sintering and it would be interesting to see if SO_2 treatment is able to promote the particle agglomeration on this type of catalysts. Finally, the SO_2 sensitivity of Pd catalysts could lead to differences in SO_2 storage and release as well as in performance.

The deactivation of DOC towards NO oxidation has been evidenced by the decrease of activity with time on stream and the lower activity during extinction yielding an inverse hysteresis. This phenomenon has been attributed to the reversible oxidation of platinum. The tendency of platinum to get oxidized varies with the nature of the support material. Platinum supported on acidic support are more resistant to oxidation, which motivated the study of acidity-enhanced Pt catalyst for DOC application.

The deposition of sulfate and chlorine in acidic solution during the preparation of Pt/Al_2O_3 was the employed method to increase the catalyst support acidity. The initial consequence of such treatment is a lower NO oxidation activity during reaction ignition but the catalysts do not exhibit deactivation during extinction. As unmodified Pt/Al_2O_3, chlorinated and sulfated catalysts were subjected to SO_2

poisoning to study the sulfur storage, the platinum sintering and the subsequent oxidation activity. Lower sulfur release was noted upon reduction of acidity-enhanced catalysts, suggesting that SO_2 storage is reduced on acidic supports. After the long SO_2 step, deactivation appeared during the cooling phase of NO oxidation. This indicates the loss of the acidic character of the catalysts, likely due to the loss of chlorine and sulfate, respectively. Further characterization of the fresh and used catalysts would be valuable. The determination of the initial and final chlorine/sulfate content as well as the trapping of released species during the flow reactor tests would enable one to correlate the chlorine/sulfate content to catalyst acidity and oxidation performance. It would also be good to evaluate Pt catalysts supported on various materials with acidic nature such as silica-alumina.

The characterization of a Cu-BEA catalyst for NH_3-SCR, following a four-step protocol, with intra-monolith spatial measurements disclosed the utilization of the catalyst for reaction and storage. NO oxidation and NH_3 oxidation were noticed at 325 and 400°C. In particular 100 % ammonia was oxidized at 400°C at the catalyst exit. However, during SCR, equal amount of ammonia and nitric oxide was consumed at any axial position in the catalyst, indicating no ammonia over-consumption and SCR stoichiometry of $NO:NH_3= 1$. Selective reduction of NO by NH_3 in lean condition is fast and uses only a limited zone in the front of the catalyst to be complete. The required zone to reach full conversion is condensed to the inlet as the operating temperature increases from 200 to 400°C. Thus at 400°C ammonia is already consumed by SCR reaction before direct ammonia oxidation becomes significant. The analysis of ammonia storage revealed that all sites within the SCR zone are filled during SCR conditions (NO, NH_3 and O_2). A kinetic model was developed based on spatially resolved steady state concentrations. The advantage of SpaciMS measurement is the possibility to collect interpretable data in realistic gas composition and temperature conditions. Indeed, conversion differences inside the monolith are observed in different conditions, even when outlet conversion is 100 %. A global kinetic model was developed and parameters were tuned to fit axial concentration profiles obtained by spatially-resolved measurement. The model used a global kinetic expression for NO oxidation and described the SCR kinetics as a reaction between adsorbed ammonia and gas phase NO. The model includes the formation of N_2O as a side product of SCR. Two mechanisms accounting for low and high temperature N_2O formation were proposed. The model agreed well with the experiment as it reproduced well the transient response to gas composition changes during the experimental protocol. In the future, the study of the Fast SCR reaction to develop further the kinetic model could be carried out. This implies overcoming the experimental difficulties of working with SpaciMS at high NO_2 concentration, due to the stickiness of this gas in the capillary probe.

List of abbreviations

DOC	Diesel Oxidation Catalyst
BET	Brunauer Emmett Teller
SCR	Selective Catalytic Reduction
HC	Hydrocarbon
TWC	Three-Way Catalyst
LNT	Lean NO_x-Trap
ASC	Ammonia Slip Catalyst
DPF	Diesel Particulate Filter
PM	Particulate Matter
TEM	Transmission Electron Microscopy
SpaciMS	Spatially-resolved Capillary Inlet Mass Spectrometer
XPS	X-ray Photoelectron Spectroscopy
TOR	Turn Over Rate
EXAFS	Extended X-ray Absorption Fine Structure
DRIFT	Diffuse Reflectance Infrared Fourier Transform
TPD	Temperature Programmed Desorption
NSR	NO_x Storage Reduction
HAADF	High Angle Annular Dark Field
STEM	Scanning Transmission Electron Microscopy
MS	Mass Spectrometer
FTIR	Fourier Transform Infra Red
CFD	Computational Fluid Dynamics
ORNL	Oak Ridge National Laboratory
TPR	Temperature-Programmed Reduction
IR	Infra Red
DC	Dynamic Capacity
UC	Unused Capacity
TC	Total Capacity
RDS	Rate Determining Step

Acknowledgments

The Swedish Foundation for Strategic Research is gratefully acknowledged for funding this project.

This work was carried out at the Competence Centre for Catalysis (KCK), Chalmers University of Technology. KCK is financially supported by Chalmers University of Technology, the Swedish Energy Agency and the member companies: AB Volvo, Volvo Car Corporation, Scania CV AB, Haldor Topsoe A/S and ECAPS AB.

I would like to thank Professor Bengt Andersson and Professor Louise Olsson for giving me the opportunity to do my PhD at Chalmers.

I would like to thank again Louise, as my supervisor, for her guidance, her support and positive attitude, for giving me the chance to visit ORNL and giving me freedom and independence in my research.

Bill Partridge and Jae-Soon Choi, my co-workers and friends from ORNL, for making my visit in Tennessee so enjoyable, for the good work we achieved and all the things I learned with you.

I would also like to thank all the colleagues who helped me through the years. I want to thank especially my friends/colleagues Slavi and Azis for their support and assistance and for all the discussions and good times.

Finally, I thank my family and friends who did not see me much in the past five years but kept supporting me.

Bibliographic references

[1] S.G. Masters, D. Chadwick, Applied Catalysis B: Environmental 23 (1999) 235-246.

[2] F.C. Meunier, J.P. Breen, V. Zuzaniuk, M. Olsson, J.R.H. Ross, Journal of Catalysis 187 (1999) 493-505.

[3] R.M. Heck, Catalysis Today 53 (1999) 519-523.

[4] J.S. Choi, W.P. Partridge, C.S. Daw, Applied Catalysis B: Environmental 77 (2007) 145-156.

[5] J. Després, M. Elsener, M. Koebel, O. Kröcher, B. Schnyder, A. Wokaun, Applied Catalysis B: Environmental 50 (2004) 73-82.

[6] S.S. Mulla, N. Chen, L. Cumaranatunge, G.E. Blau, D.Y. Zemlyanov, W.N. Delgass, W.S. Epling, F.H. Ribeiro, Journal of Catalysis 241 (2006) 389-399.

[7] S.S. Mulla, N. Chen, W.N. Delgass, W.S. Epling, F.H. Ribeiro, Catalysis Letters 100 (2005) 267-270.

[8] D. Bhatia, R.W. McCabe, M.P. Harold, V. Balakotaiah, Journal of Catalysis 266 (2009) 106-119.

[9] L. Olsson, H. Persson, E. Fridell, M. Skoglundh, B. Andersson, Journal of Physical Chemistry B 105 (2001) 6895-6906.

[10] L. Olsson, B. Westerberg, H. Persson, E. Fridell, M. Skoglundh, B. Andersson, Journal of Physical Chemistry B 103 (1999) 10433-10439.

[11] M. Crocoll, S. Kureti, W. Weisweiler, Journal of Catalysis 229 (2005) 480-489.

[12] J.H. Lee, H.H. Kung, Catalysis Letters 51 (1998) 1-4.

[13] E. Xue, K. Seshan, J.R.H. Ross, Applied Catalysis B: Environmental 11 (1996) 65-79.

[14] L. Olsson, E. Fridell, Journal of Catalysis 210 (2002) 340-353.

[15] S. Benard, L. Retailleau, F. Gaillard, P. Vernoux, A. Giroir-Fendler, Applied Catalysis B: Environmental 55 (2005) 11-21.

[16] P.J. Schmitz, R.J. Kudla, A.R. Drews, A.E. Chen, C.K. Lowe-Ma, R.W. McCabe, W.F. Schneider, C.T. Goralski Jr, Applied Catalysis B: Environmental 67 (2006) 246-256.

[17] P. Denton, A. Giroir-Fendler, H. Praliaud, M. Primet, Journal of Catalysis 189 (2000) 410-420.

[18] A. Boubnov, S. Dahl, E. Johnson, A.P. Molina, S.B. Simonsen, F.M. Cano, S. Helveg, L.J. Lemus-Yegres, J.-D. Grunwaldt, Applied Catalysis B: Environmental 126 (2012) 315-325.

[19] H.F. Wang, Y.L. Guo, G. Lu, P. Hu, Journal of Physical Chemistry C 113 (2009) 18746-18752.

[20] S.K. Matam, E.V. Kondratenko, M.H. Aguirre, P. Hug, D. Rentsch, A. Winkler, A. Weidenkaff, D. Ferri, Applied Catalysis B: Environmental 129 (2013) 214-224.

[21] K. Hauff, U. Tuttlies, G. Eigenberger, U. Nieken, Applied Catalysis B: Environmental 123-124 (2012) 107-116.

[22] W. Hauptmann, M. Votsmeier, J. Gieshoff, A. Drochner, H. Vogel, Applied Catalysis B: Environmental 93 (2009) 22-29.

[23] O. Kröcher, M. Widmer, M. Elsener, D. Rothe, Industrial and Engineering Chemistry Research 48 (2009) 9847-9857.

[24] K. Mudiyanselage, Y. Cheol-Woo, J. Szanyi, Journal of Physical Chemistry C 113 (2009) 5766-5776.

[25] S. Ovesson, B.I. Lundqvist, W.F. Schneider, A. Bogicevic, Physical Review B (Condensed Matter and Materials Physics) 71 (2005) 115406-115401.

[26] C.B. Wang, C.T. Yeh, Journal of Catalysis 178 (1998) 450-456.

[27] C.B. Wang, C.T. Yeh, Applied Catalysis A: General 209 (2001) 1-9.

[28] P. Briot, A. Auroux, D. Jones, M. Primet, Applied Catalysis 59 (1990) 141-152.

[29] R.W. McCabe, C. Wong, H.S. Woo, Journal of Catalysis 114 (1988) 354-367.

[30] H. Oh, J. Luo, W.S. Epling, Catalysis Letters 141 (2011) 1746-1751.

[31] I.V. Yentekakis, V. Tellou, G. Botzolaki, I.A. Rapakousios, Applied Catalysis B: Environmental 56 (2005) 229-239.

[32] K. Irani, W.S. Epling, R. Blint, Applied Catalysis B: Environmental 92 (2009) 422-428.

[33] L. Olsson, M. Abul-Milh, H. Karlsson, E. Jobson, P. Thormählen, A. Hinz, Topics in Catalysis 30-31 (2004) 85-90.

[34] M.F. Irfan, J.H. Goo, S.D. Kim, Environmentalist 31 (2011) 4-10.

[35] M.F. Irfan, J.H. Goo, S.D. Kim, S.C. Hong, Chemosphere 66 (2007) 54-59.

[36] H.C. Yao, H.K. Stepien, H.S. Gandhi, Journal of Catalysis 67 (1981) 231-236.

[37] A. Baylet, C. Capdeillayre, L. Retailleau, J.L. Valverde, P. Vernoux, A. Giroir-Fendler, Applied Catalysis B: Environmental 102 (2011) 180-189.

[38] S. Benard, A. Baylet, P. Vernoux, J.L. Valverde, A. Giroir-Fendler, Catalysis Communications 36 (2013) 63-66.

[39] L.M. Carballo, E.E. Wolf, Journal of Catalysis 53 (1978) 366-373.

[40] M. Haneda, T. Watanabe, N. Kamiuchi, M. Ozawa, Applied Catalysis B: Environmental 142–143 (2013) 8-14.

[41] P. Marécot, A. Fakche, B. Kellali, G. Mabilon, P. Prigent, J. Barbier, Applied Catalysis B: Environmental 3 (1994) 283-294.

[42] O. Shakir, A. Yezerets, N.W. Currier, W.S. Epling, Applied Catalysis A: General 365 (2009) 301-308.

[43] A. Russell, C. Henry, N.W. Currier, A. Yezerets, W.S. Epling, Applied Catalysis A: General 397 (2011) 272-284.

[44] J.-H. Lee, H. Kung, Catalysis Letters 51 (1998) 1-4.

[45] A. Abedi, R. Hayes, M. Votsmeier, W.S. Epling, Catalysis Letters 142 (2012) 930-935.

[46] M. Devadas, O. Kröcher, M. Elsener, A. Wokaun, N. Söger, M. Pfeifer, Y. Demel, L. Mussmann, Applied Catalysis B: Environmental 67 (2006) 187-196.

[47] M. Koebel, G. Madia, M. Elsener, Catalysis Today 73 (2002) 239-247.

[48] I. Nova, C. Ciardelli, E. Tronconi, D. Chatterjee, B. Bandl-Konrad, Catalysis Today 114 (2006) 3-12.

[49] M. Koebel, M. Elsener, M. Kleemann, Catalysis Today 59 (2000) 335-345.

[50] J.-Y. Luo, X. Hou, P. Wijayakoon, S.J. Schmieg, W. Li, W.S. Epling, Applied Catalysis B: Environmental 102 (2011) 110-119.

[51] A. Grossale, I. Nova, E. Tronconi, D. Chatterjee, M. Weibel, Journal of Catalysis 256 (2008) 312-322.

[52] T. Komatsu, M. Nunokawa, I.S. Moon, T. Takahara, S. Namba, T. Yashima, Journal of Catalysis 148 (1994) 427-437.

[53] K. Rahkamaa-Tolonen, T. Maunula, M. Lomma, M. Huuhtanen, R.L. Keiski, Catalysis Today 100 (2005) 217-222.

[54] S.J. Schmieg, S.H. Oh, C.H. Kim, D.B. Brown, J.H. Lee, C.H.F. Peden, D.H. Kim, Catalysis Today 184 (2012) 252-261.

[55] J.H. Kwak, R.G. Tonkyn, D.H. Kim, J. Szanyi, C.H.F. Peden, Journal of Catalysis 275 (2010) 187-190.

[56] J.H. Kwak, D. Tran, S.D. Burton, J. Szanyi, J.H. Lee, C.H.F. Peden, Journal of Catalysis 287 (2012) 203-209.

[57] H. Sjövall, L. Olsson, E. Fridell, R.J. Blint, Applied Catalysis B: Environmental 64 (2006) 180-188.

[58] F. Cabello Galisteo, R. Mariscal, M. López Granados, M.D. Zafra Poves, J.L.G. Fierro, V. Kröger, R.L. Keiski, Applied Catalysis B: Environmental 72 (2007) 272-281.

[59] J. Pazmiño, S. Mulla, W.N. Delgass, F.H. Ribeiro, J.T. Miller, Kinetic studies on the stability of Pt for NO oxidation: Effect of sulfur and long term aging, 2009.

[60] C.R. Apesteguia, T.F. Garetto, C.E. Brema, J.M. Parera, Applied Catalysis 10 (1984) 291-295.

[61] G. Corro, R. Montiel, C. Vázquez L, Catalysis Communications 3 (2002) 533-539.

[62] Y. Yazawa, N. Takagi, H. Yoshida, S.-i. Komai, A. Satsuma, T. Tanaka, S. Yoshida, T. Hattori, Applied Catalysis A: General 233 (2002) 103-112.
[63] K. Foger, J.R. Anderson, Applications of Surface Science 2 (1979) 335-351.
[64] I. Guo, T.T. Yu, S.E. Wanke, Changes in Pt crystallite sizes as a result of treating Pt/Al2O3 catalysts in different atmospheres, 1988, pp. 21-32.
[65] K. Foger, Catalysis : Science and technology, Springer, Verlag Berlin Heidelberg New York Tokyo, 1984.
[66] J.S. Choi, W.P. Partridge, C.S. Daw, Applied Catalysis A: General 293 (2005) 24-40.
[67] J.-S. Choi, W.P. Partridge, W.S. Epling, N.W. Currier, T.M. Yonushonis, Catalysis Today 114 (2006) 102-111.
[68] W.P. Partridge, J.S. Choi, Applied Catalysis B: Environmental 91 (2009) 144-151.
[69] W.P. Partridge, T.J. Toops, J.B. Green, T.R. Armstrong, Journal of Power Sources 160 (2006) 454-461.
[70] J. Sá, D.L.A. Fernandes, F. Aiouache, A. Goguet, C. Hardacre, D. Lundie, W. Naeem, W.P. Partridge, C. Stere, Analyst 135 (2010) 2260-2272.
[71] K. Irani, W.S. Epling, R. Blint, Topics in Catalysis 52 (2009) 1856-1859.
[72] A. Russell, W.S. Epling, H. Hess, H.Y. Chen, C. Henry, N. Currier, A. Yezerets, Industrial and Engineering Chemistry Research 49 (2010) 10311-10322.
[73] E. Ruckenstein, B. Pulvermacher, Journal of Catalysis 29 (1973) 224-245.
[74] P.C. Flynn, S.E. Wanke, Journal of Catalysis 34 (1974) 390-399.
[75] P.C. Flynn, S.E. Wanke, Journal of Catalysis 34 (1974) 400-410.
[76] P.C. Flynn, S.E. Wanke, Journal of Catalysis 37 (1975) 432-448.
[77] R.M.J. Fiedorow, S.E. Wanke, Journal of Catalysis 43 (1976) 34-42.
[78] T.J. Lee, Y.G. Kim, Journal of Catalysis 90 (1984) 279-291.
[79] J.R. Chang, S.L. Chang, T.B. Lin, Journal of Catalysis 169 (1997) 338-346.
[80] L. Olsson, H. Karlsson, Catalysis Today 147 (2009) S290-S294.
[81] M. Kärkkäinen, M. Honkanen, V. Viitanen, T. Kolli, A. Valtanen, M. Huuhtanen, K. Kallinen, M. Vippola, T. Lepistö, J. Lahtinen, R.L. Keiski, Topics in Catalysis 56 (2013) 672-678.
[82] M. Cabié, S. Giorgio, C.R. Henry, M.R. Axet, K. Philippot, B. Chaudret, The Journal of Physical Chemistry C 114 (2010) 2160-2163.
[83] A.F. Lee, K. Wilson, R.M. Lambert, C.P. Hubbard, R.G. Hurley, R.W. McCabe, H.S. Gandhi, Journal of Catalysis 184 (1999) 491-498.
[84] A. Hinz, M. Skoglundh, E. Fridell, A. Andersson, Journal of Catalysis 201 (2001) 247-257.
[85] D. Bounechada, S. Fouladvand, L. Kylhammar, T. Pingel, E. Olsson, M. Skoglundh, J. Gustafson, M. Di Michiel, M.A. Newton, P.A. Carlsson, Physical Chemistry Chemical Physics 15 (2013) 8716-8721.
[86] J.C. Summers, Environmental Science and Technology 13 (1979) 321-325.
[87] Y. Xie, Y. Chen, Y. Ma, Z. Jin, Journal of Hazardous Materials 195 (2011) 223-229.
[88] H. Wakita, Y. Kani, K. Ukai, T. Tomizawa, T. Takeguchi, W. Ueda, Applied Catalysis A: General 283 (2005) 53-61.
[89] J. Dawody, M. Skoglundh, L. Olsson, E. Fridell, Journal of Catalysis 234 (2005) 206-218.
[90] L. Limousy, H. Mahzoul, J.F. Brilhac, P. Gilot, F. Garin, G. Maire, Applied Catalysis B: Environmental 42 (2003) 237-249.
[91] R. Streber, C. Papp, M.P.A. Lorenz, O. Höfert, E. Darlatt, A. Bayer, R. Denecke, H.P. Steinrück, Chemical Physics Letters 494 (2010) 188-192.
[92] P. Zebisch, M. Stichler, P. Trischberger, M. Weinelt, H.P. Steinrück, Surface Science 371 (1997) 235-244.
[93] S.W. Nam, G.R. Gavalas, Applied Catalysis 74 (1991) 53-64.
[94] J.-Y. Luo, D. Kisinger, A. Abedi, W.S. Epling, Applied Catalysis A: General 383 (2010) 182-191.
[95] J. Li, A. Kumar, X. Chen, N. Currier, A. Yezerets, SAE Technical Papers 2 (2013).

[96] J.H. Pazmiño, J.T. Miller, S.S. Mulla, W. Nicholas Delgass, F.H. Ribeiro, Journal of Catalysis 282 (2011) 13-24.
[97] Y. Yazawa, N. Kagi, S.I. Komai, A. Satsuma, Y. Murakami, T. Hattori, Catalysis Letters 72 (2001) 157-160.
[98] Y. Yazawa, H. Yoshida, T. Hattori, Journal of Synchrotron Radiation 8 (2001) 560-562.
[99] Y. Yazawa, H. Yoshida, N. Takagi, N. Kagi, S. Komai, A. Satsuma, Y. Murakami, T. Hattori, in: F.V.M.S.M. Avelino Corma, G.F. José Luis (Eds.), Studies in Surface Science and Catalysis, Elsevier, 2000, pp. 2189-2194.
[100] I.V. Yentekakis, R.M. Lambert, M. Konsolakis, N. Kallithrakas-Kontos, Catalysis Letters 81 (2002) 181-185.
[101] M. Konsolakis, I.V. Yentekakis, Applied Catalysis B: Environmental 29 (2001) 103-113.
[102] A. Melchor, E. Garbowski, M.V. Mathieu, M. Primet, Journal of the Chemical Society, Faraday Transactions 1: Physical Chemistry in Condensed Phases 82 (1986) 3667-3679.
[103] J. Basset, F. Figueras, M.V. Mathieu, M. Prettre, Journal of Catalysis 16 (1970) 53-61.
[104] J.P. Giannetti, R.T. Sebulsky, Product R&D 8 (1969) 356-361.
[105] T. Cai, S. Liu, J. Qü, S. Wong, Z. Song, M. He, Applied Catalysis A: General 97 (1993) 113-122.
[106] T. Yamaguchi, Applied Catalysis 61 (1990) 1-25.
[107] T. Yamaguchi, T. Jin, K. Tanabe, Journal of Physical Chemistry 90 (1986) 3148-3152.
[108] O. Saur, M. Bensitel, A.B.M. Saad, J.C. Lavalley, C.P. Tripp, B.A. Morrow, Journal of Catalysis 99 (1986) 104-110.
[109] W. Przystajko, R. Fiedorow, I.G. Dalla Lana, Applied Catalysis 15 (1985) 265-275.
[110] M. Waqif, J. Bachelier, O. Saur, J.C. Lavalley, Journal of Molecular Catalysis 72 (1992) 127-138.
[111] K. Kamasamudram, N.W. Currier, X. Chen, A. Yezerets, Catalysis Today 151 (2010) 212-222.
[112] R. Nedyalkova, K. Kamasamudram, N.W. Currier, J. Li, A. Yezerets, L. Olsson, Journal of Catalysis 299 (2013) 101-108.
[113] G. Delahay, B. Coq, S. Kieger, B. Neveu, Catalysis Today 54 (1999) 431-438.
[114] A. Grossale, I. Nova, E. Tronconi, Catalysis Today 136 (2008) 18-27.
[115] M. Colombo, I. Nova, E. Tronconi, Catalysis Today 197 (2012) 243-255.
[116] P.S. Metkar, M.P. Harold, V. Balakotaiah, Chemical Engineering Science 87 (2013) 51-66.
[117] L. Olsson, H. Sjövall, R.J. Blint, Applied Catalysis B: Environmental 81 (2008) 203-217.
[118] H. Sjovall, R.J. Blint, L. Olsson, Journal of Physical Chemistry C 113 (2009) 1393-1405.
[119] H. Sjövall, R.J. Blint, A. Gopinath, L. Olsson, Industrial and Engineering Chemistry Research 49 (2010) 39-52.
[120] H. Sjövall, R.J. Blint, L. Olsson, Applied Catalysis B: Environmental 92 (2009) 138-153.
[121] E. Tronconi, I. Nova, C. Ciardelli, D. Chatterjee, B. Bandl-Konrad, T. Burkhardt, Catalysis Today 105 (2005) 529-536.
[122] N. Wilken, K. Kamasamudram, N.W. Currier, J. Li, A. Yezerets, L. Olsson, Catalysis Today 151 (2010) 237-243.
[123] S. Shwan, J. Jansson, J. Korsgren, L. Olsson, M. Skoglundh, Catalysis Today 197 (2012) 24-37.